Title: Biallelic *RIPK1* mutations in humans cause severe immunodeficiency, arthritis and intestinal inflammation

Authors: Delphine Cuchet-Lourenço[1]†, Davide Eletto[1]†, Changxin Wu[1]†#, Vincent Plagnol[2], Olivier Papapietro[1], James Curtis[1], Lourdes Ceron-Gutierrez[3], Chris M. Bacon[4,5], Scott Hackett[6], Badr Alsaleem[7], Mailis Maes[1], Miguel Gaspar[1], Ali Alisaac[1,8], Emma Goss[1], Eman AlIdrissi[9], Daniela Siegmund[10], Harald Wajant[10], Dinakantha Kumararatne[3], Mofareh S. AlZahrani[9], Peter D. Arkwright[11], Mario Abinun[12], Rainer Doffinger[3], Sergey Nejentsev[1*]

† Contributed equally

Affiliations:

[1] Department of Medicine, University of Cambridge, Cambridge, CB2 0QQ, UK.

[2] University College London Genetics Institute, University College London, London, UK

[3] Department of Clinical Biochemistry and Immunology, Addenbrooke's Hospital, Cambridge, UK

[4] Northern Institute for Cancer Research, Newcastle University, Newcastle upon Tyne, UK

[5] Department of Cellular Pathology, Newcastle upon Tyne Hospitals NHS Foundation Trust, Newcastle upon Tyne, UK

[6] Paediatric Immunology Department, Birmingham Heartland Hospital, Birmingham, UK

[7] Children's Hospital, King Fahad Medical City, King Saud bin Abdulaziz University for Health Sciences, Riyadh, Kingdom of Saudi Arabia

[8] Faculty of Applied Medical Sciences, Albaha University, Albaha, Kingdom of Saudi Arabia

[9] Children's Hospital, University of King Saud for Health Sciences, King Fahad Medical City, Riyadh, Kingdom of Saudi Arabia

[10] Division of Molecular Internal Medicine, Department of Internal Medicine II, University Hospital Würzburg, Würzburg, Germany

[11] University of Manchester, Royal Manchester Children's Hospital, Manchester, UK

[12] Primary Immunodeficiency Group, Institute of Cellular Medicine, Newcastle University, Newcastle upon Tyne, UK

Current address: Institute of Biomedical Sciences (IBMS), Shangxin University, Taiyuan, China

* Corresponding author. Email: sn262@cam.ac.uk

Abstract:

Receptor Interacting Serine/Threonine Kinase 1 (RIPK1) is a master regulator of signaling pathways leading to inflammation and cell death and is of medical interest as a drug target. Here, we report four patients from three unrelated families with complete RIPK1 deficiency caused by rare homozygous mutations. The patients suffered from recurrent infections, early-onset inflammatory bowel disease and progressive polyarthritis. They had immunodeficiency with lymphopenia and altered production of various cytokines revealed by whole-blood assays. *In vitro*, RIPK1-deficient cells showed impaired MAPK activation and cytokine secretion and were prone to necroptosis. Hematopoietic stem cell transplantation reversed cytokine production defects and resolved clinical symptoms in one patient. Thus, RIPK1 plays a critical role in the human immune system.

Main Text:

Primary immunodeficiencies (PIDs) are a heterogeneous group of disorders characterized by increased susceptibility to infections. In many cases PIDs are monogenic disorders that follow Mendelian inheritance and mutations in more than 300 genes have been shown to cause PIDs (*1*). However, in many PID patients causative mutations remain unknown. Identification of such mutations not only facilitates diagnosis of PIDs, but also can provide the fundamental knowledge about the roles of the affected proteins in the human immune system.

Here, we used exome sequencing to identify causative mutations in a heterogeneous cohort of PID patients with unknown genetic etiology (*2*). We excluded known polymorphisms (*2*) and studied rare variants. We noticed that four patients (P1 – P4) from three unrelated consanguineous families (Fig. 1A) had homozygous loss-of-function mutations in the same gene, *RIPK1* (ENST00000380409). In patients P1 and P2 from family A, the mutation was a 4-nucleotide frameshift deletion in *RIPK1* exon 6 that led to a premature stop codon (Fig. 1B). In patient P3 from family B, we found a 21-nucleotide deletion that removed one nucleotide in *RIPK1* exon 4 and 20 nucleotides in the following intron (Fig. 1B). This deletion activated an alternative splice site in intron 4, so that the *RIPK1* transcript lacked the last nucleotide of exon 4 and had an insertion of 48 nucleotides from the following intron (fig. S1). Patient P4 from family C had a homozygous 2,064-nucleotide deletion that completely removed *RIPK1* exon 4 (Fig. 1B and fig. S2). Parents of all patients were heterozygous carriers of these *RIPK1* mutations (Fig. 1A and fig. S3). Given that homozygous loss-of-function mutations in the *RIPK1* gene had never been reported in humans (e.g., absent from more than 120,000 subjects in the gnomAD database (*3*)), such mutations in our patients are likely to be pathogenic. The *RIPK1* gene encodes a 671 amino-acid serine/threonine kinase (Fig. 1C). All three mutations mapped to the N-terminal kinase domain and produced premature stop codons. The RIPK1 protein was absent in cells of patients P2, P3 and P4 (Fig. 1D). Therefore, all three homozygous mutations led to complete RIPK1 deficiency. The four patients had lymphopenia, suffered from recurrent viral, bacterial and fungal infections, early-onset inflammatory bowel disease (IBD) involving upper and lower gastrointestinal tract and developed arthritis (Tables S1 and S2, fig. S4 and Supplementary Text (*2*)). Therefore, these clinical features characterize RIPK1 deficiency in humans.

RIPK1 is a widely expressed cytosolic protein kinase controlling multiple signaling pathways leading to inflammation and apoptotic or necroptotic cell death (*4, 5*). RIPK1 is present in protein complexes that mediate signal transduction from cell surface receptors, including TNFR1, TLR3 and TLR4 (*4, 5*). Stimulation of these receptors activates the canonical NF-κB pathway and the mitogen-activated protein kinases (MAPKs). This leads to phosphorylation of NF-κB and AP-1 transcription factors, which induces expression of pro-inflammatory and pro-survival genes (*4, 6*). To assess the functioning of these signaling pathways, we stimulated patients' skin fibroblasts with TNFα and poly(I:C) *in vitro*. We found that phosphorylation of MAPK p38 and the AP-1 subunit cJun was markedly reduced (Fig. 2A and fig. S5), while phosphorylation of MAPK p42/44 (ERK2/1) and NF-κB p65 was partially reduced (fig. S6). TNFα-induced secretion of cytokines IL-6 and RANTES by patients' fibroblasts was also diminished (fig. S7). Thus, similar to studies in RIPK1-deficient mice (*7-11*), pro-inflammatory signaling downstream of TNFR1 and TLR3 is impaired in the patients. We next investigated whether RIPK1 deficiency affected cell viability. After stimulation with TNFα or poly(I:C), we found significantly fewer viable fibroblasts of patients than those of healthy controls ($P < 0.001$; Fig. 2B). When we transduced patient's fibroblasts and expressed wild-type RIPK1, this viability defect was reversed (fig. S8) and activation of the MAPK and NF-κB pathways was also rescued (fig. S9). To investigate the mechanism of cell death, we studied patient's fibroblasts 24 hours after poly(I:C) stimulation and found increased phosphorylation of RIPK3 and Mixed Lineage Kinase Domain Like Pseudokinase (MLKL), proteins that mediate necroptosis (*12, 13*) (Fig. 2C). No cleavage of caspase-8 and minimal cleavage of caspase-3 were found, indicating that apoptosis was not a major death mechanism of these cells (fig. S10). Consistent with these results, MLKL inhibitor Necrosulfonamide and,

to a lesser extent, RIPK3 inhibitor GSK′872 rescued patient's cells from poly(I:C)-induced death, while pan-caspase inhibitor zVAD-fmk had no effect (Fig. 2D). As expected, RIPK1 inhibitors Nec-1s and GSK2982772 had no effect on these RIPK1-deficient cells (Fig. 2D).

To investigate the molecular basis of the immune dysfunction responsible for the disease, we studied cytokine release in whole blood assays. After stimulation with phytohemagglutinin (PHA), patients' blood cells produced markedly increased amounts of IL-1β (Fig. 3A). This enhanced IL-1β response to PHA normalized in patient P2 after hematopoietic stem cell transplantation (HSCT) (Fig. 3A). Also, after PHA stimulation patients' blood produced reduced amounts of IL-17 and IFN-γ, while the production of TNFα, IL-6 and IL-10 was similar to controls (fig. S11), which shows dysregulated but not generally suppressed responses of stimulated T cells. After stimulation with lipopolysaccharide (LPS), whole blood of healthy controls produced large amounts of IL-6 and IL-10 and showed strongly up-regulated production of TNFα and IL-12 upon co-stimulation with LPS and IFN-γ (Fig. 3B). These responses were dramatically reduced in the RIPK1-deficient patients, but normalized in patient P2 after HSCT (Fig. 3B). At the same time, we found normal production of IL-10, IL-6 and TNFα in patients' whole blood assays after stimulation with TLR1/2 and TLR2/6 ligands Pam3CSK4 and Pam2CSK4 (fig. S12), consistent with the RIPK1-independent signaling downstream of these receptors (*4*). The production of IL-1β in whole blood of the patients was within normal range after LPS stimulation and was slightly reduced after LPS and IFN-γ co-stimulation (fig. S13). Similar to whole blood assays, primary monocytes isolated from blood of patient P4 and stimulated with LPS showed reduced production of IL-6, TNFα and IL-12 (Fig. 3C). However, the production of IL-1β was increased (Fig. 3C).

We next analyzed in more detail the response of RIPK1-deficient human immune cells to LPS stimulation. We were unable to conduct further studies of primary blood cells from the patients because P1 and P3 had died, P2 had undergone HSCT and P4 was not available. We therefore used CRISPR-Cas9 technology to knock out RIPK1 in the human monocyte-like THP-1 cell line (*2*). After LPS stimulation, THP-1$^{RIPK1-/-}$ cells secreted reduced amounts of IL-6 and IL-10 and released increased amounts of IL-1β (Fig. 3D), resembling the cytokine response of patients' cells (Fig. 3C). The impaired cytokine production was preceded by the reduced phosphorylation of MAPK p38 (Fig. 3E), mirroring the defective MAPK p38 phosphorylation in the patients' primary fibroblasts (Fig. 2A). Activation of NF-κB p65 and other branches of the MAPK pathway was not affected in the THP-1$^{RIPK1-/-}$ cells (fig. S14). Differential activation of the MAPK and NF-κB pathways after LPS stimulation was reported previously (*14*), and our results indicate that RIPK1 deficiency in THP-1 cells preferentially alters LPS-induced MAPK p38 activation.

After LPS stimulation, THP-1$^{RIPK1-/-}$ cells showed increased phosphorylation of RIPK3 and MLKL and enhanced cell death (Figs. 3F and 3G). No cleavage of caspase-8 or caspase-3 was found (fig. S15). Necrosulfonamide and GSK′872, but not zVAD-fmk, reduced death of THP-1$^{RIPK1-/-}$ cells (Fig. 3G), again pointing at necroptosis as the main death mechanism of these cells. Necroptosis of THP-1$^{RIPK1-/-}$ cells was accompanied by the release of cleaved caspase-1 that we found in the supernatant together with IL-1β (Fig. 3H), suggesting concurrent activation of inflammasome. Next, we compared mechanisms that mediate IL-1β release from LPS-stimulated THP-1$^{RIPK1-/-}$ cells with those that mediate IL-1β release during pyroptosis of wild-type THP-1 cells stimulated by LPS and Nigericin. We found that different mechanisms are at play. After treatment with Necrosulfonamide, IL-1β release during

pyroptosis was only slightly reduced, while it was completely prevented in THP-1$^{RIPK1-/-}$ cells, suggesting that in these cells IL-1β release is secondary to necroptosis (fig. S16). Of note, treatment of THP-1$^{RIPK1-/-}$ cells with Necrosulfonamide did not restore reduced IL-6 secretion (fig. S17), indicating that it is reduced not because of enhanced necroptosis, but is an earlier phenomenon. Taken together, these data show that human RIPK1-deficient cells have impaired pro-inflammatory signaling leading to dysregulated cytokine secretion and are prone to necroptosis, which, in myeloid cells, is accompanied by IL-1β release.

RIPK1 has been extensively studied in mouse models (*7-9, 15-18*) and its inhibitors are considered for the treatment of acute and chronic organ injury, including stroke, myocardial infarction and renal ischemia–reperfusion injury (*19*, *20*), but the phenotype associated with RIPK1 deficiency in humans was unknown. While the *Ripk1*-knockout mice displayed systemic inflammation and cell death in multiple tissues and died during the postnatal period (*7-9*), the clinical presentation of our RIPK1-deficient patients was less severe. Nevertheless, they suffered from immunodeficiency, gut inflammation and progressive polyarthritis. During infection, activation of the pattern-recognition receptors TLR3 and TLR4 and stimulation of TNFR1 by secreted TNFα induces pro-inflammatory effects. Consistent with the established role of RIPK1 in the signal-transducing protein complexes assembled downstream of these receptors (*4-7, 10, 11*), we found impaired pro-inflammatory signaling in RIPK1-deficient cells and reduced production of multiple cytokines. These defects, as well as lymphopenia, likely explain susceptibility to infections in the patients.

Our data show that LPS stimulation of RIPK1-deficient monocytes resulted in the increased necroptosis and IL-1β release, similar to the previous observation in the RIPK1-deficient monocytes transdifferentiated from immortalized human B cells (*21*). Furthermore,

we found high IL-1β levels after PHA stimulation of the patients' whole blood. This may suggest that IL-1β production by T cells, which was reported recently (*22, 23*), is also increased in the context of RIPK1 deficiency. Alternatively, dysregulated secretion of T cell factors after PHA stimulation may have augmented the IL-1β production by patients' monocytes in whole blood. IL-1β is a pro-inflammatory cytokine involved in the pathogenesis of arthritis and IBD (*24, 25*). Another cytokine dysregulated in our patients, IL-10, is essential for balancing immune response in the gut and impaired signaling in the IL-10 pathway has been associated with IBD (*26, 27*). Therefore, it is likely that low secretion of IL-10 and increased IL-1β production contributed to the pathogenesis of arthritis and IBD in our RIPK1-deficient patients. Accordingly, treatment with IL-1 inhibitors may be considered in RIPK1 deficiency, although none of our patients received such therapy. Interestingly, while patients P1, P2 and P3 developed severe IBD in the first months of life, P4 had no IBD signs up until the age of 4 years. Therefore, genetically determined RIPK1 deficiency was not the sole cause of IBD in these patients. Rather, it led to the dysregulated cytokine production, which set the immune system in a predisposition mode, while additional factors, e.g. distinct microbiomes, likely affected progression to IBD in these patients. This scenario resembles the adult-onset IBD, where immune predisposition is determined by multiple common genetic polymorphisms, while progression to clinical disease is driven by environmental factors (*28*).

The intestinal epithelium provides a physical barrier and participates in maintaining immune homeostasis in the gut. Mice genetically deficient in *Ripk1* in the intestinal epithelial cells (IEC) developed severe lethal intestinal pathology due to FADD–caspase-8-mediated apoptosis of IEC (*9, 29*). Histological examination of gastrointestinal biopsies from P1 and P2 showed only occasional cells with apoptotic morphology and cells positive for cleaved

caspase-3 (fig. S18). Such cells were also present in biopsies from children with idiopathic IBD and histologically normal biopsies (fig. S18). Thus, in contrast to the mouse model, no extensive IEC apoptosis was found, suggesting that it is not a characteristic feature of RIPK1 deficiency in humans. Likewise, skin disorders were not typical in our patients, indicating no special protective role of human RIPK1 in keratinocytes, in contrast to mice with epidermis-specific RIPK1 knockout that developed severe skin inflammation (*9, 30*). Given that HSCT in patient P2 resolved IBD and arthritis and reduced the frequency of infections (*2*), it is likely that dysfunction of the immune system rather than dysfunction of other cell types was critical for disease development.

In summary, our findings indicate that RIPK1 has a more narrow function in humans than in mice, with the effects of RIPK1 deficiency being largely confined to the immune system. Accordingly, HSCT performed at young age can be an effective treatment in RIPK1-deficient patients.

References and notes:

1. A. Bousfiha *et al.*, The 2017 IUIS Phenotypic Classification for Primary Immunodeficiencies. *J Clin Immunol* **38**, 129 (2018).
2. Materials and Methods are available as Supplementary Materials.
3. M. Lek *et al.*, Analysis of protein-coding genetic variation in 60,706 humans. *Nature* **536**, 285 (2016).
4. D. Ofengeim, J. Yuan, Regulation of RIP1 kinase signalling at the crossroads of inflammation and cell death. *Nat Rev Mol Cell Biol* **14**, 727 (2013).

5. M. Pasparakis, P. Vandenabeele, Necroptosis and its role in inflammation. *Nature* **517**, 311 (2015).

6. M. Najjar *et al.*, RIPK1 and RIPK3 Kinases Promote Cell-Death-Independent Inflammation by Toll-like Receptor 4. *Immunity* **45**, 46 (2016).

7. M. A. Kelliher *et al.*, The death domain kinase RIP mediates the TNF-induced NF-kappaB signal. *Immunity* **8**, 297 (1998).

8. J. A. Rickard *et al.*, RIPK1 regulates RIPK3-MLKL-driven systemic inflammation and emergency hematopoiesis. *Cell* **157**, 1175 (2014).

9. M. Dannappel *et al.*, RIPK1 maintains epithelial homeostasis by inhibiting apoptosis and necroptosis. *Nature* **513**, 90 (2014).

10. T. H. Lee *et al.*, The death domain kinase RIP1 is essential for tumor necrosis factor alpha signaling to p38 mitogen-activated protein kinase. *Mol Cell Biol* **23**, 8377 (2003).

11. E. Meylan *et al.*, RIP1 is an essential mediator of Toll-like receptor 3-induced NF-kappa B activation. *Nat Immunol* **5**, 503 (2004).

12. D. W. Zhang *et al.*, RIP3, an energy metabolism regulator that switches TNF-induced cell death from apoptosis to necrosis. *Science* **325**, 332 (2009).

13. L. Sun *et al.*, Mixed lineage kinase domain-like protein mediates necrosis signaling downstream of RIP3 kinase. *Cell* **148**, 213 (2012).

14. R. A. Gottschalk *et al.*, Distinct NF-kappaB and MAPK Activation Thresholds Uncouple Steady-State Microbe Sensing from Anti-pathogen Inflammatory Responses. *Cell Syst* **2**, 378 (2016).

15. K. Newton *et al.*, Activity of protein kinase RIPK3 determines whether cells die by necroptosis or apoptosis. *Science* **343**, 1357 (2014).

16. A. Polykratis *et al.*, Cutting edge: RIPK1 Kinase inactive mice are viable and protected from TNF-induced necroptosis in vivo. *J Immunol* **193**, 1539 (2014).

17. W. J. Kaiser *et al.*, RIP1 suppresses innate immune necrotic as well as apoptotic cell death during mammalian parturition. *Proc Natl Acad Sci U S A* **111**, 7753 (2014).

18. J. E. Roderick *et al.*, Hematopoietic RIPK1 deficiency results in bone marrow failure caused by apoptosis and RIPK3-mediated necroptosis. *Proc Natl Acad Sci U S A* **111**, 14436 (2014).

19. A. Degterev *et al.*, Chemical inhibitor of nonapoptotic cell death with therapeutic potential for ischemic brain injury. *Nat Chem Biol* **1**, 112 (2005).

20. H. Zhao *et al.*, Role of necroptosis in the pathogenesis of solid organ injury. *Cell Death Dis* **6**, e1975 (2015).

21. M. M. Gaidt *et al.*, Human Monocytes Engage an Alternative Inflammasome Pathway. *Immunity* **44**, 833 (2016).

22. B. N. Martin *et al.*, T cell-intrinsic ASC critically promotes T(H)17-mediated experimental autoimmune encephalomyelitis. *Nat Immunol* **17**, 583 (2016).

23. G. Arbore *et al.*, T helper 1 immunity requires complement-driven NLRP3 inflammasome activity in CD4(+) T cells. *Science* **352**, aad1210 (2016).

24. G. Schett, J. M. Dayer, B. Manger, Interleukin-1 function and role in rheumatic disease. *Nat Rev Rheumatol* **12**, 14 (2016).

25. M. F. Neurath, Cytokines in inflammatory bowel disease. *Nat Rev Immunol* **14**, 329 (2014).

26. R. Kuhn, J. Lohler, D. Rennick, K. Rajewsky, W. Muller, Interleukin-10-deficient mice develop chronic enterocolitis. *Cell* **75**, 263 (1993).

27. E. O. Glocker *et al.*, Inflammatory bowel disease and mutations affecting the interleukin-10 receptor. *N Engl J Med* **361**, 2033 (2009).

28. B. Khor, A. Gardet, R. J. Xavier, Genetics and pathogenesis of inflammatory bowel disease. *Nature* **474**, 307 (2011).

29. N. Takahashi *et al.*, RIPK1 ensures intestinal homeostasis by protecting the epithelium against apoptosis. *Nature* **513**, 95 (2014).

30. J. Lin *et al.*, RIPK1 counteracts ZBP1-mediated necroptosis to inhibit inflammation. *Nature* **540**, 124 (2016).

31. The 1000 Genomes Project Consortium, An integrated map of genetic variation from 1,092 human genomes. *Nature* **491**, 56 (2012).

32. W. Fu *et al.*, Analysis of 6,515 exomes reveals the recent origin of most human protein-coding variants. *Nature* **493**, 216 (2013).

33. V. Plagnol *et al.*, A robust model for read count data in exome sequencing experiments and implications for copy number variant calling. *Bioinformatics* **28**, 2747 (2012).

34. C. Zheng, B. J. Baum, All human EF1alpha promoters are not equal: markedly affect gene expression in constructs from different sources. *Int J Med Sci* **11**, 404 (2014).

35. E. J. Schatorje *et al.*, Paediatric reference values for the peripheral T cell compartment. *Scand J Immunol* **75**, 436 (2012).

ACKNOWLEDGMENTS

We thank S. Prothero, who participated in the patients' treatment. **Funding**: S.N. was supported by the Wellcome Trust (095198/Z/10/Z), MRC (MR/M012328/1) and the ERC Starting grant (260477). S.N., D.K., and R.D. are supported by the National Institute for Health

Research (NIHR) Cambridge Biomedical Research Centre. H.W. is supported by the Deutsche Forschungsgemeinschaft (WA 1025/31-1). This work was also supported by the MRC/EPSRC Newcastle Molecular Pathology Node. **Author contributions:** D.C.-L., D.E., C.W., O.P., M.M., M.G., A.A., E.G., D.S. and H.W. performed cell experiments and analyzed the data. V.P. analyzed exome data. J.C. performed sequencing. M.A., P.D.A., M.S.AlZ., D.K., E.AlI., B.A. and S.H. looked after the patients and collected patients' data. C.M.B. analyzed biopsies. R.D. and L.C.-G. performed cytokine analyses. S.N. planned the experiments, analyzed the data and wrote the first draft of the manuscript. **Competing interests:** Authors declare no competing interests. **Data and materials availability:** Cells are available upon signing a Material Transfer Agreement. Sequence data for the *RIPK1* gene region are available in Sequence Read Archive under the accession number SRP136541. Whole exome data are available upon signing a Data Transfer Agreement.

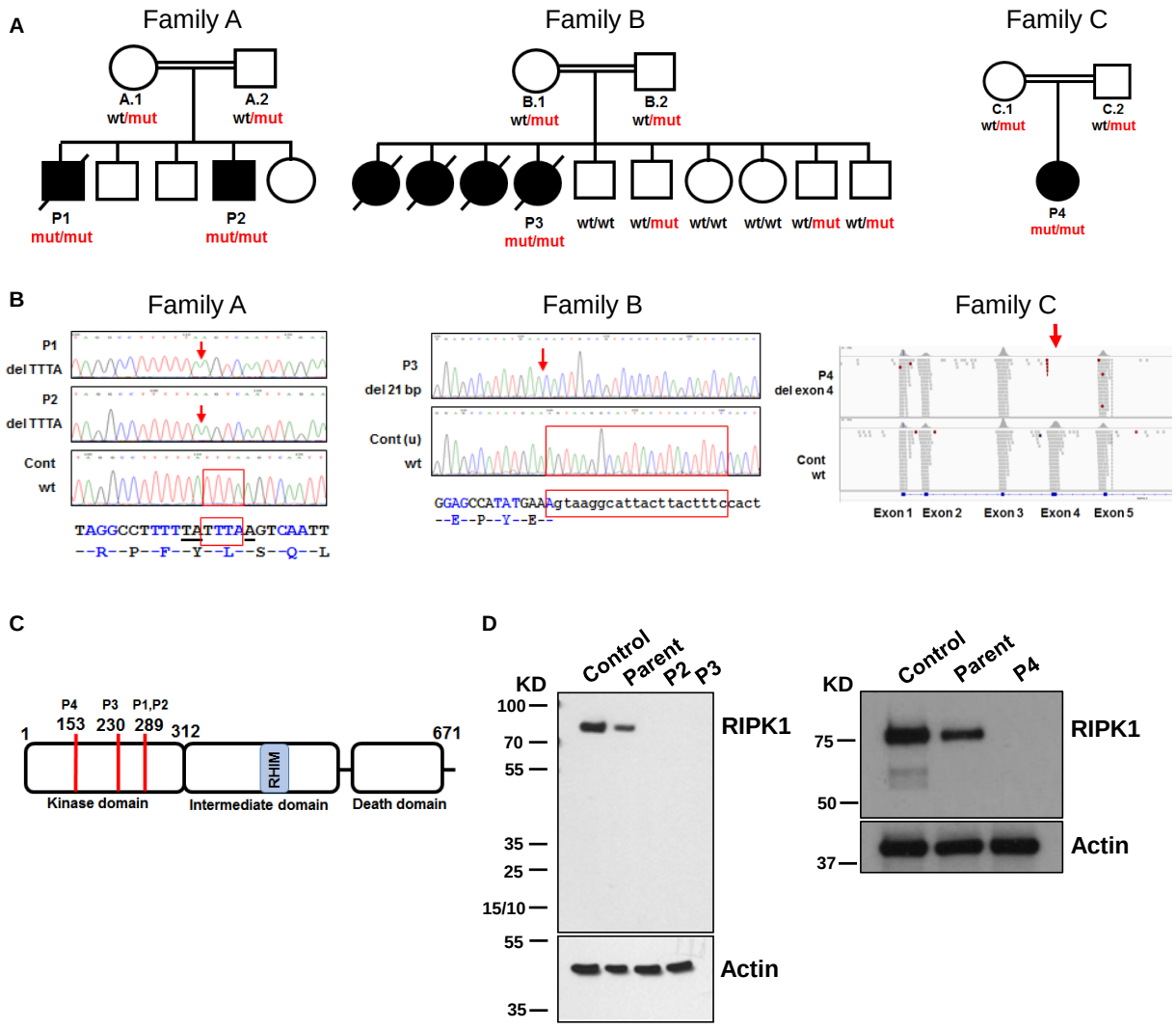

Fig. 1. Mutations of the *RIPK1* gene cause complete RIPK1 deficiency

(A) Three families with the *RIPK1* gene mutations: wt, wild-type allele; mut, mutant allele. ○ and □ - unaffected; ● and ■ - affected. **(B)** Patients' mutations. Locations of deletions are shown by red arrows; deleted nucleotides are shown by red frames. Deletion of exon 4 in P4 (right panel). **(C)** Domains of the RIPK1 protein. RHIM - Receptor-interacting protein (RIP) Homotypic Interaction Motif. Codons affected by mutations are shown by red lines; codon numbers and corresponding patients are indicated above. **(D)** Western blot assays for detection of RIPK1 protein in fibroblasts (left panel) and T cell blasts (right panel).

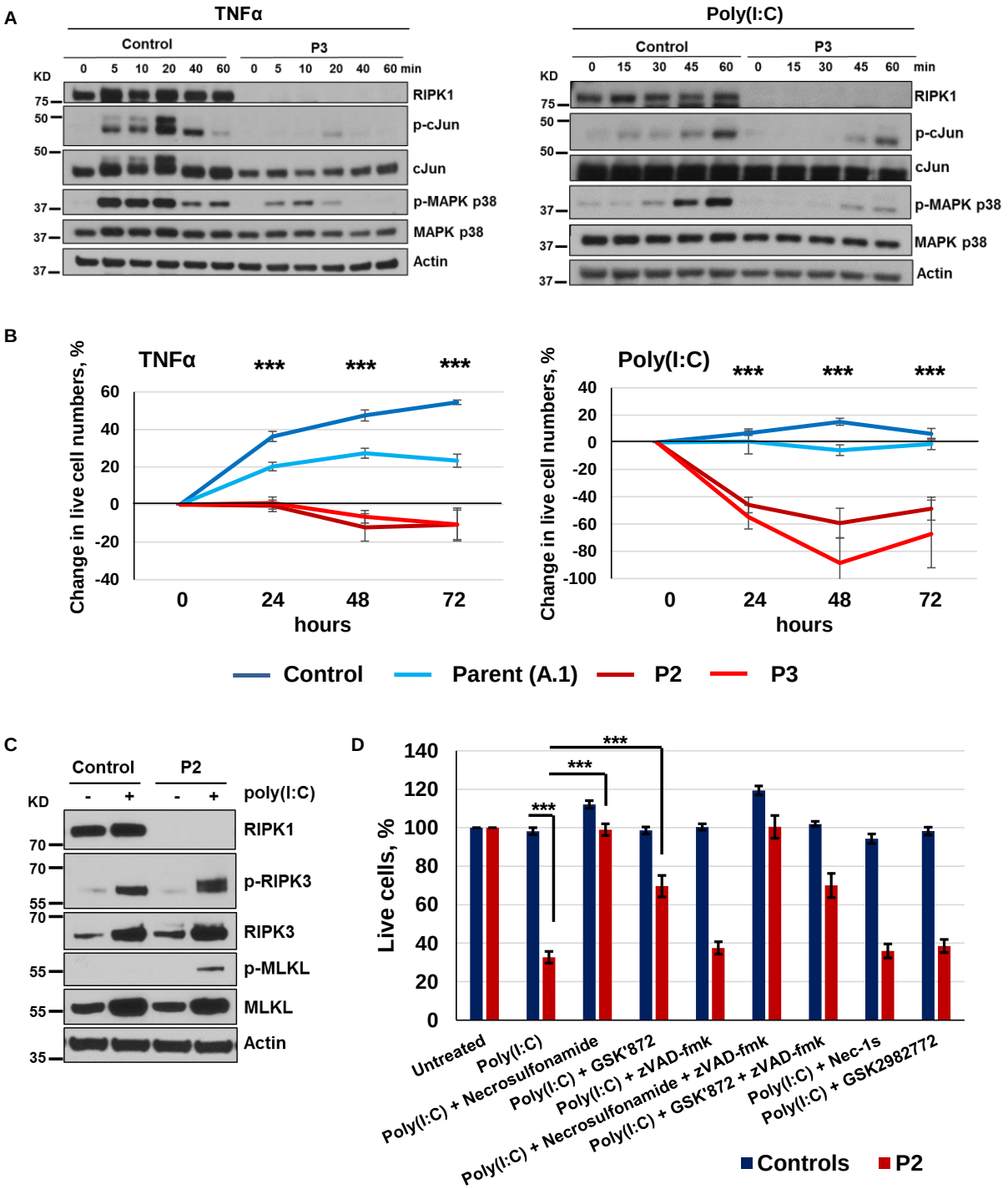

Fig. 2. RIPK1-deficient fibroblasts show impaired MAPK signaling and necroptosis

(A) Primary fibroblasts were stimulated with 50 ng/mL TNFα or 100 µg/mL poly(I:C) and protein extracts were subjected to immunoblotting (N = 2). **(B)** Viability of primary fibroblasts after stimulation with 100 ng/mL TNFα or 20 µg/mL poly(I:C). Experiments were repeated at

least three times. Differences between stimulated and unstimulated cells are shown at each time point relative to the 0 time point. *P*-values were calculated using two-tailed unpaired T-test, comparing combined data from healthy subjects (parent and control) vs patients (P2 and P3); graphs show mean values ± SEM. **(C)** Fibroblasts were stimulated with 20 μg/mL poly(I:C) for 24 hours and protein extracts were subjected to immunoblotting (N = 1). **(D)** Fibroblasts of P2 and controls (unrelated and parent A.1) were stimulated with 20 μg/mL poly(I:C) for 24 hours in the presence of indicated compounds and cell viability was measured ($N \geq 6$); graphs show mean values ± SEM. *P*-values were calculated using two-tailed unpaired T-tests. *** $P < 0.001$.

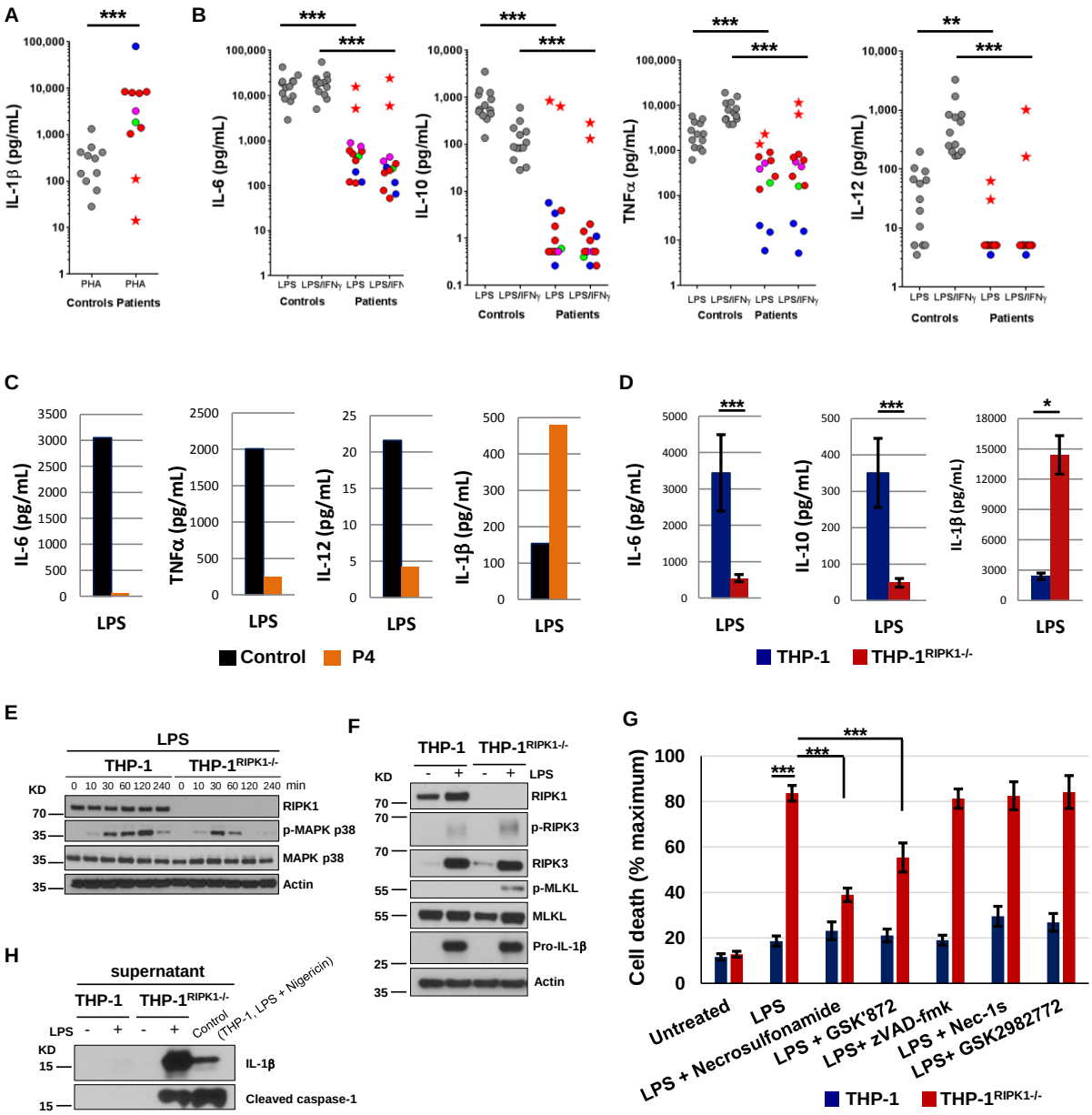

Fig. 3. RIPK1-deficient immune cells show dysregulated cytokine production, impaired MAPK signaling and necroptosis

(A-B) Cytokines were measured in whole blood after 24 hours stimulation using 10 µg/mL PHA **(A)** or 1 µg/mL LPS or 1 µg/mL LPS plus 20,000 IU/mL IFN-γ **(B)**. To account for lymphopenia data were corrected for lymphocyte counts. Controls are shown as grey circles, patients as colored circles (P1 – magenta, P3 – blue, P4 – green, P2 before HSCT – red); P2

after HSCT – red star. *P*-values were calculated using two-tailed Mann-Whitney test, excluding the data of P2 after HSCT. **(C)** CD14+ monocytes were purified from PBMC of patient P4 (age 3 y) and a healthy adult (travel control), stimulated overnight with 5 μg/mL LPS and then cytokines were measured in supernatants. N = 1, two technical replicates, graphs show mean values. **(D)** THP-1 cells (2 wild-type and 7 THP-$1^{RIPK1-/-}$ clones) were treated with 50 ng/mL phorbol 12-myristate 13-acetate (PMA) for 3 days, rested for 1 day and stimulated overnight with 5 μg/mL LPS. Cytokines were measured in supernatants. The data were corrected for the estimated number of live cells and show means combining data for different clones ± SEM. *P*-values were calculated using two-tailed unpaired T-test. **(E)** THP-1 cells were treated with PMA as in (D), stimulated with 1 μg/mL LPS and the extracted proteins were analyzed by immunoblotting (N = 2). **(F)** THP-1 cells were stimulated with 5 μg/mL LPS for 48 hours and the extracted proteins were analyzed by immunoblotting (N = 2). **(G)** THP-1 cells were stimulated with 5 μg/mL LPS for 48 hours in the presence of indicated compounds and cell death was measured using lactate dehydrogenase (LDH) release assay ($N \geq 4$). The data show means ± SEM. *P*-values were calculated using two-tailed unpaired T-test. **(H)** Supernatants of THP-1 cells studied in (F) were analyzed by immunoblotting (N = 1). * $P < 0.05$, ** $P < 0.01$, *** $P < 0.001$.

Supplementary Materials

Materials and Methods

Supplementary Text

Tables S1 to S2

Figures S1 to S18

References (31-35)

Supplementary Materials for

Biallelic *RIPK1* mutations in humans cause severe immunodeficiency, arthritis and intestinal inflammation

Delphine Cuchet-Lourenço, Davide Eletto, Changxin Wu, Vincent Plagnol, Olivier Papapietro, James Curtis, Lourdes Ceron-Gutierrez, Chris M. Bacon, Scott Hackett, Badr Alsaleem, Mailis Maes, Miguel Gaspar, Ali Alisaac, Emma Goss, Eman AlIdrissi, Daniela Siegmund, Harald Wajant, Dinakantha Kumararatne, Mofareh S. AlZahrani, Peter D. Arkwright, Mario Abinun, Rainer Doffinger, Sergey Nejentsev

correspondence to: sn262@cam.ac.uk

This PDF file includes:

Materials and Methods

Primary immunodeficiency (PID) patients

The PID cohort consisted of 48 patients that suffered severe and/or disseminated and/or recurrent bacterial and/or viral infections and have been diagnosed with common variable immunodeficiency (CVID), specific antibody deficiency with poor vaccine responses, combined T and B-cell immunodeficiencies, phagocyte and innate immunity defects, as well as undefined PIDs. The nature and possible consequences of the study were explained to the participants and all material was obtained with informed consent in accordance with the Declaration of Helsinki and with approvals from the ethics committees (04/Q0501/119, 10/H0906/22 and 15/WS/0019).

Exome sequencing and bioinformatics analysis

We isolated DNA samples from blood or peripheral blood mononuclear cells (PBMCs). Library preparation, exome capture and sequencing have been done according to the manufacturers' instructions. For exome target enrichment Agilent SureSelect 38 Mb kit was used. Sequencing was done using Illumina HiSeq 2000. FASTQ files were aligned to the hg19 reference sequence using Novoalign version 2.07.19, including hard and soft clipping, quality calibration and adapter trimming. Duplicate reads were excluded using the PICARD tool MarkDuplicates. Calling was performed using SAMtools v0.18 and single sample calling. The resulting calls were annotated with the software ANNOVAR. Candidate variants were filtered based on function: loss-of-function, non-synonymous or potential splicing altering variants (defined as being with 5 bp of the actual splice site) and frequency. To identify rare variants, we excluded known polymorphisms previously detected in 1000 Genomes (*31*) and 6,500 exomes (*32*). To identify large deletions and duplications we used software ExomeDepth (*33*) (http://cran.r-project.org/web/packages/ExomeDepth/index.html).

RIPK1 gene mutations sequencing

To study the *RIPK1* gene mutations by Sanger sequencing we first used primers 5'CTTTGCCCACAGATTGAGGT3' and 5'TGAAGGAGAAATGGGTCCAG3' to amplify gene region with the 4-nucleotide deletion and primers 5'TTTCCTGGGCGACATTTTAC3' and 5'ACCCTGGAATTTCACAGCAC3' to amplify gene region with the 21-nucleotide deletion. We then sequenced the amplicons using one of the primers.
To study deletion of the *RIPK1* exon 4 we used PCR with flanking primers 5'TGGAAAAGGCGTGATACACA3' and 5'TGGCCTGTTCCCAGATTTTA3' and ran PCR products on an agarose gel.

To sequence cDNA of P3, initially total RNA was extracted using RNeasy mini kit (74106, Qiagen) from primary dermal fibroblasts of P3. Then, cDNA was generated using Maxima Reverse Transcriptase (EP0741, Thermo Scientific) and oligo(dT)18 primers (S0132, Thermo Scientific) according to manufacturer recommendations. Part of the *RIPK1* cDNA was amplified using primers 5'CTGAATGACGTCAACGCAAA3' and 5'AGGCTGTTCTGTGGCTGAAT3' and then sequenced using one of the primers.

Cells

Human primary dermal fibroblasts of patients, a heterozygous parent (A.1), and a healthy adult control (HDFa, C0135C, ThermoFisher Scientific, UK) as well as 293T cells were cultured in DMEM (61965-026, Gibco, Life Technologies, UK) supplemented with 10% heat-inactivated fetal bovine serum (FCS-SA/500, Labtec), 20 μM HEPES buffer (H0887, Sigma, UK), and 100 U/mL penicillin and 100 μg/mL streptomycin (P0781, Sigma, UK).

THP-1 cells were cultured in RPMI medium 1640 (21875, Gibco, life technologies, UK) with 10% heat-inactivated fetal bovine serum, 20 μM HEPES buffer, and 100 U/mL penicillin and 100 μg/mL streptomycin. When PMA differentiation was used, THP-1 cells were plated at 5 x 10^4 cells per well in 96 well plates and cultured for 3 days with 50 ng/mL PMA (Calbiochem, 524400), washed 3 times with PBS and cultured for an additional day in media without PMA before been treated as required.

Human PBMC were isolated from fresh peripheral blood by centrifugation with a gradient of Ficoll-paque Plus (17-1440-03, GE Healthcare, UK) at 2000 rpm for 23 minutes at room temperature. Buffy coat layer containing PBMC was washed with PBS 3 times. Monocytes were isolated by magnetic cell sorting using anti-CD14-coated beads (130-050-201, Miltenyi Biotec, UK). Monocytes were cultured in RPMI medium 1640 (21875, Gibco, life technologies, UK) with 10% heat-inactivated fetal bovine serum, 20 μM HEPES buffer, penicillin (100 U/ml) and streptomycin (100 μg/ml) in 48 well plates (2.8 x 10^5 cell in 250 μL per well) for 16 hours.

To generate T blasts, frozen monocyte-depleted PBMCs of patient P4 and its travel control were stimulated with Dynabeads Human T-Activator CD3/CD28 (11161D, ThermoFisher), 1 bead per cell, followed by 4 days resting in the presence of 100 U/mL IL-2.

Cloning

cDNA from primary fibroblasts of a healthy subject was amplified by PCR using the following primers:
Hind_RIPK1_cDNA_Fw 5'CCCAAGCTTATGCAACCAGACATGTCC3';
Xho_RIPK1_cDNA_Rv 5'CCGCTCGAGGTTCTGGCTGACGTAAATCAAG3'. A HindIII/XhoI double digested insert was sub-cloned into pcDNA6/myc-His A (#V22120, ThermoFisher). To generate a lentiviral vector that ensures expression in primary cells, pLJM1-EGFP (#19319, AddGene) was engineered by replacing the CMV promoter with the human elongation factor 1α (EF1α) promoter (*34*). The pcDNA6 construct served as a template for PCR amplification to introduce the FLAG-tag at the N-terminus of the RIPK1 protein (NheI_FLAG-RIPK1_Fw, 5'-CTAGCTAGC atg GACTACAAAGACGAT GACGACAAGCAACCAGACATGTCCTTGAATG – 3'; EcoRI_RIPK1_Rv, 5'CCGGAATTC tta TTCTGGCTGACGTAAATCAAGCTGC3'. The NheI/EcoRI double digested fragment was finally cloned into pEF1α-Lenti-EGFP, in place of EGFP. No mutations were found by Sanger sequencing.

Transduction of primary fibroblasts

The lentivirus stocks were prepared by transient transfection of 3 million 293T cells with the envelope plasmid pCMV-VSV-G (1 μg, AddGene #8454), the packing plasmid psPAX2 (1.4

μg, AddGene # 12260) and the expression plasmid pEF1α-Lenti -GFP or pEF1α-Lenti -FLAG-RIPK1 (2 μg) along with 13.5 μL of the transfection reagent Lipofectamine 2000 (#11668019, ThermoFisher) following the manufacturer's instructions. The following morning the media was replaced. The medium was harvested at 48 hours post transfection, cleared by low-speed centrifugation (1200 rpm, 5 min), and filtered through 0.45 μm pore size filters. Fresh collected virus stocks were used for transduction experiments. Transductions of the patient and control fibroblasts were carried out by infection in the presence of 8 μg/ml of Polybrene (107689, Sigma). 48 hours later the virus-containing media was replaced by fresh media containing 1 μg/mL of puromycin. Two to 3 days later the selected positive transduced cells were amplified and kept in the presence of 0.25 μg/mL of puromycin.

Generation of the RIPK1-knockout THP-1 cells

First, LentiCas9-Blast vector (Addgene, plasmid #52962) was used to generate THP-1 cells stably expressing Cas9. Lentiviral particles were produced as described above and then used to transduce THP-1 cells that were seeded at 5 x 10^4 cells/mL. Two days post-transduction, the cells were subjected to blasticidin selection at a concentration of 5 μg/mL for 7 days. Surviving cells were subjected to limiting dilution and plated in 96-well cell plates to obtain single clones stably expressing Cas9. After approximately 3 - 4 weeks of clonal expansion, clones were screened for Cas9 expression level by western blotting. Clones expressing Cas9 were then selected and expanded.

Then, a guide RNA (gRNA) targeting unique sequence of the *RIPK1* exon 2 was designed: CTTCCTCTATGATGACGCCCAGG. This guide was cloned into the BsmBI unique site of the LentiGuide-Puro plasmid (Addgene plasmid #52963). The constructed vector was used to produce lentiviral particles as described above. The Cas9-expressing THP-1 cells were then transduced and 48 hours later the media was replaced by fresh media containing 3 μg/mL of puromycin. Two weeks later, puromycin-resistant cells were seeded as single cells into 96-well plates for clonal expansion in the presence of conditional media (25%), high serum (20%) and anti-oxidants (20 nM BCS and 50 μM 1-Thioglycerol, B1125 and M6145, Sigma). After expansion, efficient knockout of the *RIPK1* gene in each isolated single-cell clone was confirmed by western blotting analyzing RIPK1 protein expression. In the following experiments we analyzed RIPK1-knockout ($RIPK1^{-/-}$) clones and treated them as biological replicates.

Western blotting

Unstimulated or stimulated fibroblasts, THP-1 cells or T blasts were lysed with ice-cold RIPA lysis buffer x2 (R0278, Sigma) supplemented with proteasome inhibitor (cOmplete Mini, Roche, 11836153001) for 15 min. Lysates were centrifuged at 13,000 rpm for 10 min at 4°C. Three microliters of the supernatant were used to quantify the proteins (23227, BCA assay kit, Pierce) as recommended by the supplier. The remaining supernatant was incubated with x2 Laemmli sample buffer (BIO-RAD, 161-0737), containing 2-mercaptoethanol (Sigma M7522), at 100°C for 5 min. 7.5-40 μg of proteins were resolved on 10% or 12% Acrylamide/bis gels (161-0173 and 161-0175, BIO-RAD) and transferred to PVDF membranes (170-4159, BIO-RAD) using the trans-blot turbo transfer system (1704150, BIO-RAD) and probed with the following antibodies: RIPK1 (Cell Signaling, #3493, 1 in 1,000 dilution; targeting epitope around Leu190); β-Actin (Sigma, A5441, 1 in 50,000 dilution); NF-κB p65 (Cell Signaling,

#4764, 1 in 1000 dilution); Phospho-NF-κB p65 (Cell Signaling, #3033, 1 in 1,000 dilution); c-Jun (Cell Signaling, #9165, 1 in 1,000 dilution); Phospho-c-Jun II (Cell Signaling, #9261, 1 in 1,000 dilution), p38 MAPK (Cell Signaling, #9219S, 1 in 1,000 dilution); Phospho-p38 MAPK (Cell Signaling, #4511S, 1 in 1,000 dilution); p42/44 MAPK (Cell Signaling, #4696S, 1 in 2,000 dilution); Phospho-p42/44 MAPK (Cell Signaling, #4370P, 1 in 1,000 dilution); IκBα (Cell Signaling, #4814, 1 in 1000 dilution); Phospho-IKKα/β (Cell Signaling, #2697, 1 in 1000 dilution); MLKL (Abcam, ab183770, 1 in 1,000 dilution); Phospho-MLKL (Abcam, ab187091, 1 in 1,000 dilution); RIPK3 (Cell Signaling, #13526, 1 in 1000 dilution); Phospho-RIPK3 (Cell Signaling, #93654, 1 in 1000 dilution); caspase-1 (p20) (AdipoGen Life Sciences, AG-20B-0048, 1 in 1000 dilution); caspase-3 (Cell Signaling, #9662, 1 in 1000 dilution); caspase-8 (Cell Signaling, #9746, 1 in 1000 dilution); IL-1β (R&D SYSTEMS, AF-201-NA, 1 in 1000 dilution) and GFP (Abcam, ab290, 1 in 1,000 dilution). Band densitometry was determined by ImageJ.

To study proteins released in supernatants, THP-1 cells were stimulated either with 5 μg/mL LPS for 48 hours or co-stimulated with 5 μg/mL LPS for 48 hours and 20 μM Nigericin (InvivoGen, NIG-38-02) for the last 90 minutes. To extract proteins, cell supernatants were collected and subjected to protein precipitation using methanol (v/v). Western blotting was then performed as described above.

Cell viability/proliferation and LDH release assays

Fibroblasts were seeded in completed media without antibiotics at 10,000 cells per well in 96-well plates in duplicates. The following day (0 time point), the cells were washed 3 times using PBS and treated with 100 μL of starving media without antibiotics supplemented with TNFα (final concentration 100 ng/mL) or poly(I:C) (final concentration 20 μg/mL) in the presence or absence of zVAD-fmk (BD Biosciences, 550377, final concentration 20 μM), Nec-1s (7-Cl-O-Nec-1, Calbiochem, 504297, final concentration 10 μM), GSK2982772 (Axon, 2713, final concentration 1μM), Necrosulfonamide (Calbiochem, 480073, final concentration 0.5 μM), GSK'872 (Calbiochem, 530389, final concentration 1.5 μM). DMSO (Sigma, D2438, 0.1 μg/mL) was used as a negative control. Metabolic activity of live cells was assessed at 0, 24 hours, 48 hours and 72 hours post treatment using the Promega CellTiter 96 AQueous Non-Radioactive Cell Proliferation Assay (G5421) according to the manufacturer's instructions. Each result was an average of two measurements. Statistical analysis was done using an unpaired two-tailed T-test assuming equal variance comparing cells of patients and controls.

The wild-type THP-1 cells (two parental Cas9-expressing THP-1 cell clones) and the RIPK1$^{-/-}$ THP-1 cell clones were seeded at 50,000 cells per well in 96 well plates in triplicates in completed media. Cells were stimulated with crude LPS (final concentration 5 μg/mL) in the presence or absence of zVAD-fmk (final concentration 20 μM), Nec-1s (final concentration 10 μM), GSK2982772 (final concentration 1μM), Necrosulfonamide (final concentration 0.5 μM), GSK'872 (final concentration 3 μM). DMSO (Sigma, D2438, 0.1 μg/mL) was used as a negative control. Cell death was calculated by measuring Lactate Dehydrogenase (LDH) in cell supernatants using CytoTox 96 (non-radioactive cytotoxicity assay, Promega, G1780). The absorbance was recorded at 490 nm using a micro-plate reader. The basal level of LDH release was determined with 40 μL supernatant from media and the maximal LDH release was determined with 40 μL supernatant from lysed non treated cells. The calculation of the

percentage of LDH release was as follows: 100 * (LDH release from treated group minus basal release) / (maximal LDH release minus basal release). Each result was an average of three measurements. Statistical analysis was done using an unpaired two-tailed T-test assuming equal variance comparing the wild-type THP-1 clones against the THP-1$^{RIPK1-/-}$ clones.

Cytokine production assays

Whole blood was diluted 1:5 in RPMI into 96-well F plates (Corning) and activated by single stimulation with phytohemagglutinin (PHA; 10 μg/ml; Sigma-Aldrich), LPS (1 μg/ml, List Biochemicals) or co-stimulating with LPS and IFN-γ (2 x 10^4 IU/mL, Imukin, Boehringer Ingelheim), Pam2CSK4 (1 μg/mL) or Pam2CSK4 (1 μg/mL) plus IFN-γ (2 x 10^4 IU/ml), Pam3CSK4 (1 μg/mL) or Pam3CSK4 (1 μg/mL) plus IFN-γ (2 x 10^4 IU/ml). Supernatants were taken after 24 hours. Cytokines were measured using standard ELISA according to the manufacturer's recommendations (IFN-γ, Pelikine, Sanquin, NL), or multiplexed (TNFα, IL-12, IL-10, IL-6, R+D Systems Fluorokinemap) on a Luminex analyzer (Bio-Plex, Bio-Rad, UK). Statistical analysis was done using two-tailed Mann-Whitney tests. Supernatants from primary monocytes, fibroblasts or THP-1 cells were collected 16-24 after treatment and cytokine amounts were measured using ELISA, as above. Statistical analyses were done using two-tailed unpaired T tests assuming equal variance.

Immunohistochemistry

Immunohistochemical staining of patient and control gastrointestinal biopsies was performed on formalin-fixed paraffin-embedded tissue sections using the Ventana Discovery Ultra automated platform. The following antibodies were used: cleaved caspase-3 (R&D Systems, rabbit monoclonal antibody, 269518), CD3 (Leica, mouse monoclonal antibody, LN10), and cytokeratin (Ventana, mouse monoclonal antibody cocktail, AE1/AE3 and PCK26). Antigen retrieval used the Ventana CC1 cell conditioning buffer and diaminobenzidine (DAB) detection used Ventana ultraView reagents.

Supplementary Text

Clinical and immunological findings in patients P1 – P4

In family A, parents were first cousins of Pakistani descent living in the UK. They had two affected male children, P1 and P2; two male siblings and one female sibling were healthy (Fig. 1A). In the first months of life P1 was diagnosed with perinatal human cytomegalovirus (HCMV) infection, had enteropathy with diarrhea, vomiting, hepatosplenomegaly, and failure to thrive. He developed recurrent mouth ulcers and perianal abscesses. Biopsies taken in the first year of life showed gastritis, partial villous atrophy in the duodenum and mild active chronic inflammation in the colon. Biopsies taken at the age of 4 and 12 years showed active chronic gastritis, mild chronic duodenitis and focally ulcerative active chronic inflammation in the colon (fig. S4A-C), indicating inflammatory bowel disease (IBD). Beginning in early childhood, he suffered from recurrent oral and perianal candidiasis and recurrent respiratory infections. *Mycobacterium avium intracellulare* was grown from sputum of P1 on one occasion at the age of 4 years. At 8 years of age he developed progressive erosive polyarticular arthritis. By the age of 9 years, he was diagnosed with chronic lung disease, bronchiectasis, and *Pseudomonas aeruginosa* colonization. Lung function tests showed forced expiratory volume FEV_1 and forced vital capacity (FVC) at 50-60% of normal. At the age of 11 years P1 had severe pneumonia caused by varicella zoster virus (VZV), necessitating admission to pediatric intensive care. At the age of 11 years he developed an urticarial skin rash and skin biopsy showed dermal lymphocytic vasculitis. Variable T cell lymphopenia and reduced numbers of NK cells were found (Table S2). T cell proliferation in response to mitogens, neutrophil oxidative burst and levels of immunoglobulins were normal.

Patient P2, a younger brother of P1, also had hepatosplenomegaly and enteropathy with diarrhea, perianal abscesses and anal fistula in the first months of life. Endoscopy showed IBD with persistent active chronic inflammation in the stomach, duodenum and colon (fig. S4D-F). He suffered from multiple respiratory infections, including severe respiratory syncytial virus (RSV) bronchiolitis. By the age of 32 months diarrhea continued, he developed polyarthritis, and was diagnosed with bronchiectasis. Immunological analysis showed variable CD4+ T lymphopenia, normal T cell proliferation in response to mitogens, normal levels of immunoglobulins and normal neutrophil oxidative burst (Table S2).

In family B, the parents were first cousins of the Arabic descent living in Saudi Arabia (Fig. 1A). They had 10 children, of which 3 daughters died at the age of 6 to 12 months with profuse bloody diarrhea. Patient P3, also female, presented with intractable inflammatory enteropathy with bloody diarrhea and mouth ulcers starting soon after birth. Her symptoms were only partly controlled by oral and intravenous pulses of prednisolone and anti-TNF therapy (adalimumab). At the age of four years she developed a perianal abscess requiring surgical drainage. Endoscopic and histological abnormalities were found throughout the bowel involving esophagus, stomach, small and large intestine with active inflammation characterized by microulceration of the superficial epithelium, cryptitis and crypt abscesses (fig. S4H). T lymphopenia developed from the 1^{st} year of life. She also suffered from a non-erosive inflammatory arthritis affecting hips, elbows, knees, wrists and ankles. From the age of 11 years P3 suffered from recurrent HSV infections, which led to a non-granulomatous inflammation and complete destruction of her nasal septum. At the age of 13 years she suffered from pneumonia and *Aspergillus flavus* was isolated from a bronchoalveolar lavage fluid. Her growth was below the 0.4^{th} centile for her age. At this age laboratory investigations revealed

generalized lymphopenia and hypogammaglobulinemia (Table S2). Neutrophil oxidative burst test was normal.

In family C, the parents were first cousins of the Arabic descent living in Saudi Arabia. At the age of 4 months patient P4, a female, had severe RSV bronchiolitis requiring PICU admission. Since then she had recurrent discharging otitis media treated with antibiotics and mild occasional diarrhea. IVIG was started at the age of 5 months. While P4 was on IVIG, otitis became less frequent. The patient displayed a failure to thrive, which continued at the age of 26 months despite high caloric diet. At the age of 2 years she developed arthritis of small joints of hand and knee that improved after treatment with non-steroidal anti-inflammatory drugs. Initially, she had T and NK lymphopenia, which normalized later (Table S2). Genetic analysis discovered RIPK1 deficiency in P4 when she was 3 years old. Given the history of IBD in other RIPK1-deficient patients, endoscopy was performed on P4. Normal mucosa was found in the esophagus, stomach and duodenum. Colonoscopy showed normal mucosa, except telangiectasia at a localized area in the descending colon. There was no bleeding. Colon biopsy showed normal mucosa. Thus, at the age of 3 years P4 had no IBD signs. However, at the age of 4 years P4 developed chronic bloody diarrhea with anal fissure and perianal fistula. Biopsy of rectal mucosa showed granulation tissue, indicative of ulceration, and chronic inflammation (fig. S4I). Therefore, P4 progressed to develop IBD, similarly to the other three patients.

None of the patients was treated with IL-1 inhibitors, e.g. anakinra or canakinumab. Hematopoietic stem cell transplantation (HSCT) was performed in patients P1, P2 and P3. P1 received a transplant from a 10/12 HLA-matched unrelated donor. He died at the age of 12 years, six weeks after HSCT, due to multiorgan failure including cardiac, respiratory and renal dysfunction, and encephalopathy. P3 died at the age of 13 years, three weeks after HSCT, due to disseminated HSV and adenovirus infections despite peri-transplant prophylaxis with aciclovir for HSV and cidofovir for adenovirus. P2 had HSCT from an 11/12 HLA-matched unrelated donor at the age of 30 months. Five years post-HSCT he is developing well with 100% donor chimerism in all three tested lines (myeloid CD15+, T cell CD3+ and B cell CD19+). His weight is on the 50^{th} centile, he has no diarrhea, his perianal abscesses have healed and endoscopy showed significant improvement of gut mucosa and no inflammation (fig. S4G). There is no active on-going arthritis. However, P2 remains on antibiotic prophylaxis because of the chronic lung disease and bronchiectasis.

Table S1. Summary of clinical phenotype of patients with complete RIPK1 deficiency

Patient (year of birth / gender)	Family (ethnic origin)	Infections	Arthritis, age of onset	IBD, age of onset	Lymphopenia	Outcome (age at HSCT)
P1 (1998 / M)	Family A (Pakistani)	Recurrent respiratory infections, bronchiectasis, persistent HCMV, VZV pneumonia, lung infections with *M. avium intracellulare*, *P. aeruginosa*, recurrent oral and perianal candidiasis	Polyarthritis, 9 y	First months of life	T and NK cell lymphopenia	Died post-HSCT (12 y)
P2 (2009 / M)	Family A (Pakistani)	Multiple respiratory infections, severe RSV bronchiolitis	Polyarthritis, 2 y	First months of life	CD4+ T lymphopenia	Alive and well 5 years post-HSCT (2 y 6 m)
P3 (1998 / F)	Family B (Arabic)	Recurrent HSV1 infections, Aspergillus pneumonia	Polyarthritis, 4 y	First months of life	T lymphopenia (1 y); T, B and NK lymphopenia (13 y)	Died post-HSCT (13 y)
P4 (2013 / F)	Family C (Arabic)	Severe RSV bronchiolitis, recurrent otitis media	Arthritis of small joints of hand and knee, 2 y	4 y	T, B and NK lymphopenia (3 m)	Alive, on IVIG

HCMV - human cytomegalovirus; HSCT - hematopoietic stem cell transplantation; HSV-1 - herpes simplex virus 1; IVIG - intravenous immunoglobulin; RSV - respiratory syncytial virus; IBD - inflammatory bowel disease; VZV - varicella-zoster virus.

Table S2. Immunological data of the RIPK1-deficient patients

Patient (age)	P1 (11 years)	P1 (12 years)	P2 (8 months)	P2 (2 years)	P3 (13 years)	P4 (3 months)	P4 (2 years)
Cell subsets, cells/µl (normal ranges)							
Neutrophils	5,650 (1,800-7,700)		11,300 (1,500-8,500)	3,290 (1,500-8,500)	2,600 (1,800-7,700)	15,140 ↑ (1,000-8,500)	4,070 (1,500-8,500)
Monocytes	430 (200-800)		1,250 (700-1,500)	800 (700-1,500)	1,060 (100 – 1,300)	1,450 (700-1,500)	1,020 (700-1,500)
Lymphocytes	**699** ↓ (1,400-4,200)	**1,327** ↓ (1,400-4,200)	2,900 (1,800-18,700)	3,890 (1,400-5,500)	**420** ↓ (1,400-4,200)	**1,006** ↓ (3,400-12,200)	3,100 (1,400-5,500)
T cells	**414** ↓ (850-3,200)	1,049 (850-3,200)	1,423 (1,400-11,500)	2,056 (850-4,300)	**220** ↓ (850-3,200)	**630** ↓ (2,200-9,200)	2,300 (850-4,300)
CD4+ T cells	**185** ↓ (400-2,100)	446 (400-2,100)	**898** ↓ (1,000 -7,200)	1,052 (500-2,700)	**53** ↓ (400-2,100)	**430** ↓ (1,600-6,500)	1,400 (500-2,700)
CD8+ T cells	**198** ↓ (300-1,300)	537 (300-1,300)	433 (200-5,400)	793 (200-1,800)	**111** ↓ (300-1,300)	**160** ↓ (300-3,400)	600 (200-1,800)
CD4+ naïve T cells	**79** ↓ (200-1,700)	231 (200-1,700)	**626** ↓ (800-7,600)	740 (300-2,300)	**17** ↓ (200-1,700)		
CD4- naïve T cells	**62** ↓ (78-640)	168 (78-640)	313 (150-3,200)	678 (53-1,100)	**58** ↓ (78-640)		
CD4- effector T cells	29 (16-810)	105 (16-810)	**0** ↓ (8-1,400)	**0** ↓ (24-590)	**0** ↓ (16-810)		
NK cells	**28** ↓ (92-1,200)	**38** ↓ (92-1,200)	529 (68-3,900)	347 (61-510)	**29** ↓ (92-1,200)	**40** ↓ (97-1,990)	210 (61-510)
B cells	253 (120-740)	231 (120-740)	1,133 (130-6,300)	1,477 (180-1,300)	**24** ↓ (120-740)	**390** ↓ (520-2,300)	520 (180-1,300)
T cell proliferation to PHA	normal		normal		normal	low, 58%	
Serum immunoglobulins, g/L (normal ranges)							
IgM	0.5 (0.5-1.8)	0.53 (0.5-1.8)	1.5 (0.6-2.1)	0.91 (0.4-1.8)	< **0.1** (0.5-1.8)	1.6 (0.6-2.1)	1.4 (0.4-1.8)
IgG	12.8 (4.9-16.1)	16.5 (4.9-16.1)	9.4 (3.0-10.9)	8.0 (4.5-9.1)	8.68* (4.9-16.1)	5.2 (3.0-10.9)	6.3* (4.5-9.1)
IgA	1.9 (0.7-2.5)	3.28 (0.7-2.5)	0.97 (0.4-2.0)	0.65 (0.2-1.0)	< **0.07** (0.7-2.5)	0.4 (0.4-2.0)	0.8 (0.2-1.0)
Specific antibodies (normal ranges)							
Tetanus, IU/mL	0.2(0.1-10)		2.5 (0.1-10)			**0.003** ↓(0.1-10)	
Haemophilus influenza B, mg/L	**0.2** ↓(1-20)		9 (1-20)			**0.64** ↓(1-20)	
Pneumococcus, mg/L	19(20-200)		75 (20-200)				

* on immunoglobulin replacement therapy; PHA – phytohemagglutinin. Values below normal ranges are shown in bold.
Normal ranges for T lymphocyte subsets are from (*35*)

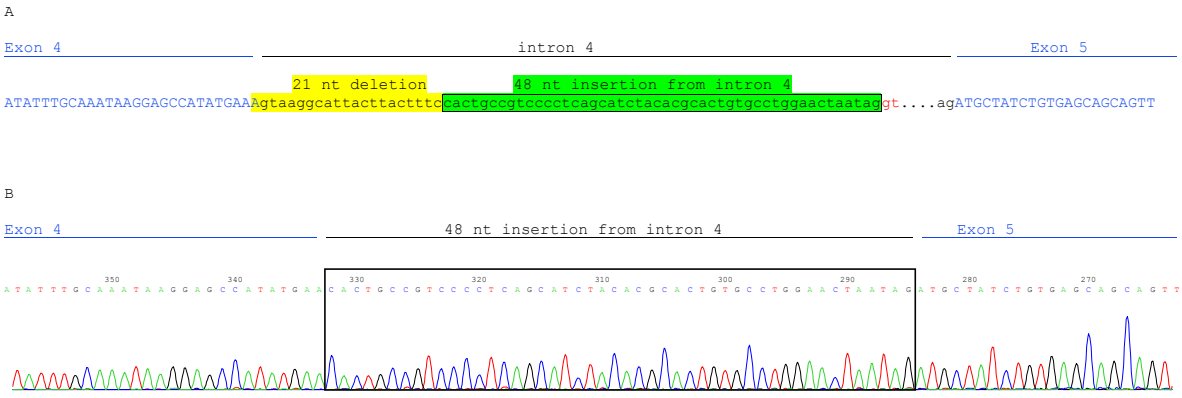

Fig. S1. Mutation found in patient P3
(A) Schematic presentation of the mutation. DNA sequences of the *RIPK1* exons 4 and 5 are shown in upper case; DNA sequence of intron 4 is shown in lower case. The 21-nucleotide deletion in the patient's DNA is highlighted in yellow, including one base of exon 4 and twenty bases of intron 4. The 48-nucleotide insertion from intron 4 in the patient's cDNA is highlighted in green. The activated cryptic slice site in intron 4 is shown in red. Irrelevant part of intron 4 is shown by dots.
(B) Electropherogram of the patient's cDNA showing sequences matching to exon 4 (excluding one last nucleotide A), 48-nucleotide insertion from intron 4 and then exon 5.

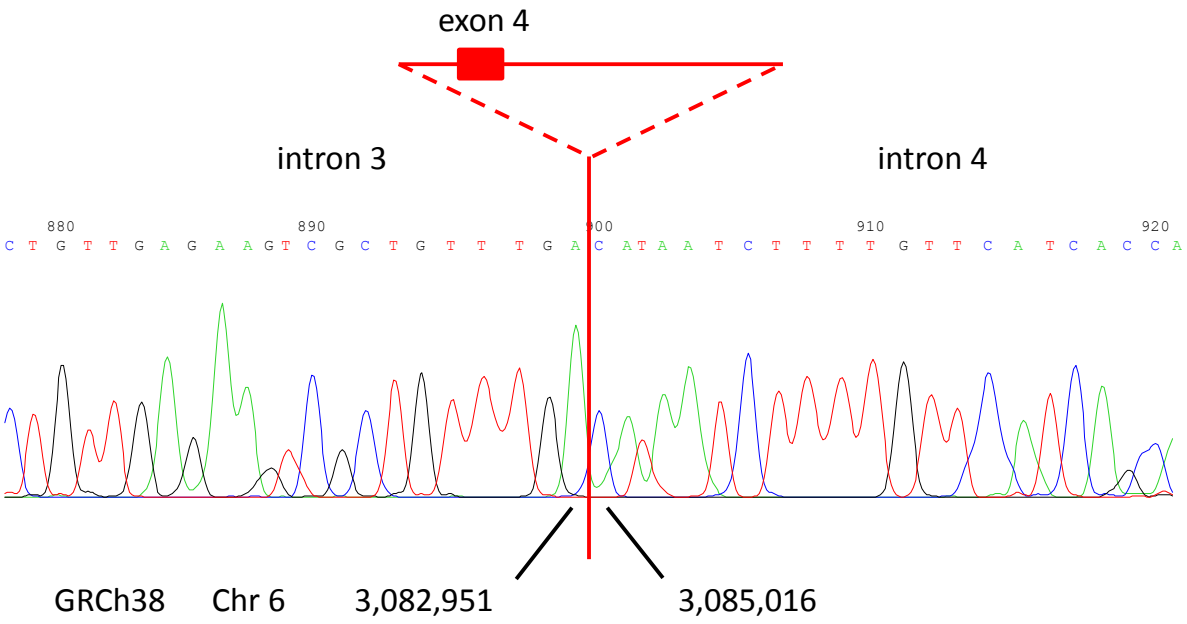

Fig. S2. Mutation found in patient P4
Electropherogram of the patient's DNA with sequences matching to introns 3 and 4 showing a 2,064-nucleotide deletion. Nucleotide positions of the deletion breakpoints in the GRCh38 genome build are shown below.

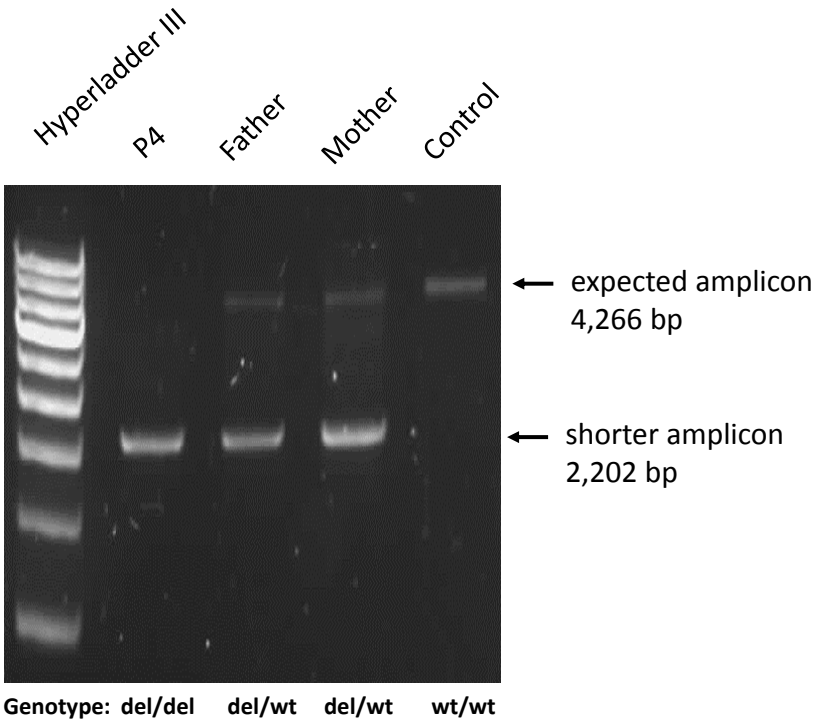

Fig. S3. PCR flanking the 2,064-nucleotide deletion found in family C
Gel electrophoresis shows an amplicon of the expected size in control; a shorter amplicon due to deletion is present in patient P4; both amplicons are present in heterozygous parents. del – deletion, wt – wild type.

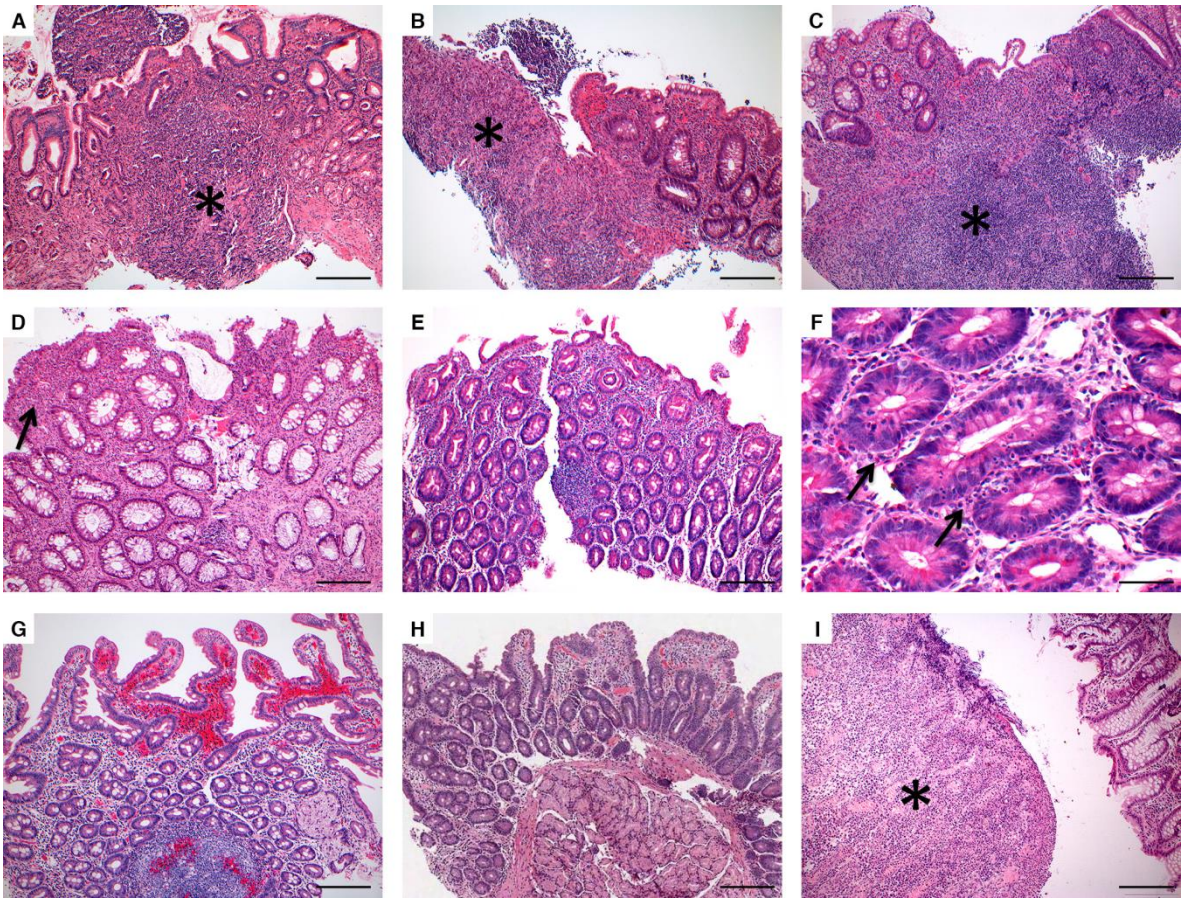

Fig. S4. Gastrointestinal tract biopsies of patients P1- P4
Hematoxylin and eosin staining.
(A) Stomach of P1showing active chronic inflammation including a prominent lymphoid aggregate in the gastric mucosa (asterisk). Scale bar = 200 μm.
(B) Colon of P1 showing active chronic inflammation with patchy ulceration (asterisk). Scale bar = 200 μm.
(C) Colon of P1 showing active chronic inflammation with large lymphoid aggregates in mucosa and submucosa (asterisk). Scale bar = 200 μm.
(D) Rectum of P2 showing chronic inflammatory changes including branching crypts, fibrosis and Paneth cell metaplasia. There is an increase in chronic inflammatory cells and foci of acute inflammation (arrow). Scale bar = 200 μm.
(E) Duodenum of P2 showing marked villous atrophy, crypt hyperplasia and an increase in chronic inflammatory cells in the lamina propria. Scale bar = 200 μm.
(F) Duodenum of P2 at higher magnification showing patchy acute inflammation of crypt epithelium (arrow). Scale bar = 50 μm.
(G) Duodenum of P2, 10 months after HSCT, showing a substantially improved villous architecture with no significant inflammation. Scale bar = 200 μm.
(H) Small intestine of P3 showing distortion of villous architecture with short and blunted villi and patchy crypt hyperplasia. A focal increase in acute inflammatory cells was observed. Scale bar = 200 μm.
(I) Rectum of P4 showing granulation tissue (asterisk), indicative of ulceration, overlying mucosa showing mild chronic inflammatory changes. Scale bar = 200 μm.

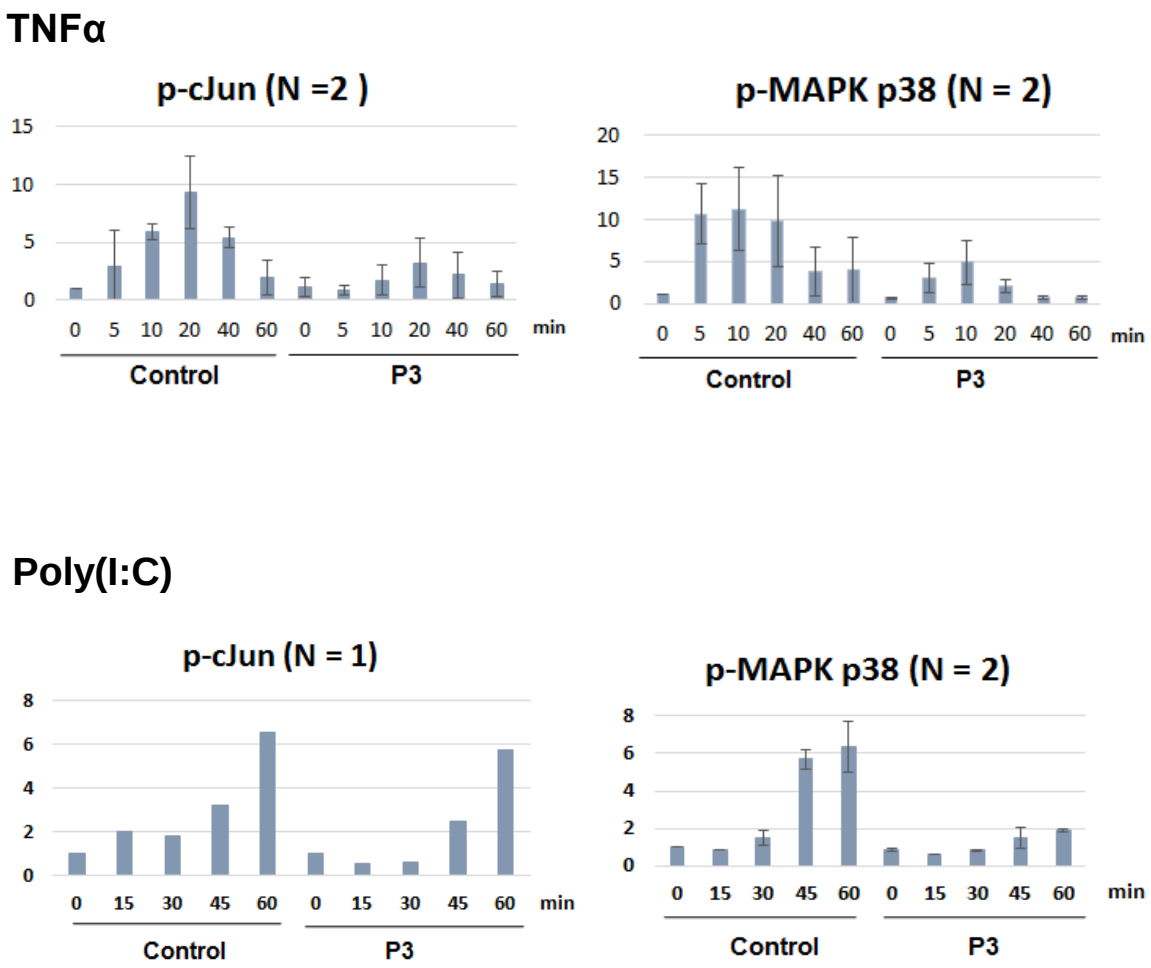

Fig. S5. RIPK1-deficient fibroblasts show reduced phosphorylation of MAPK p38 and cJun

Primary fibroblasts were stimulated with 50 ng/mL TNFα or 100 μg/mL poly(I:C) and protein extracts were subjected to immunoblotting as shown in Fig. 2A. Bar graphs show fold change of band densitometry. N shows the number of independent experiments. Graphs show mean values ± SD.

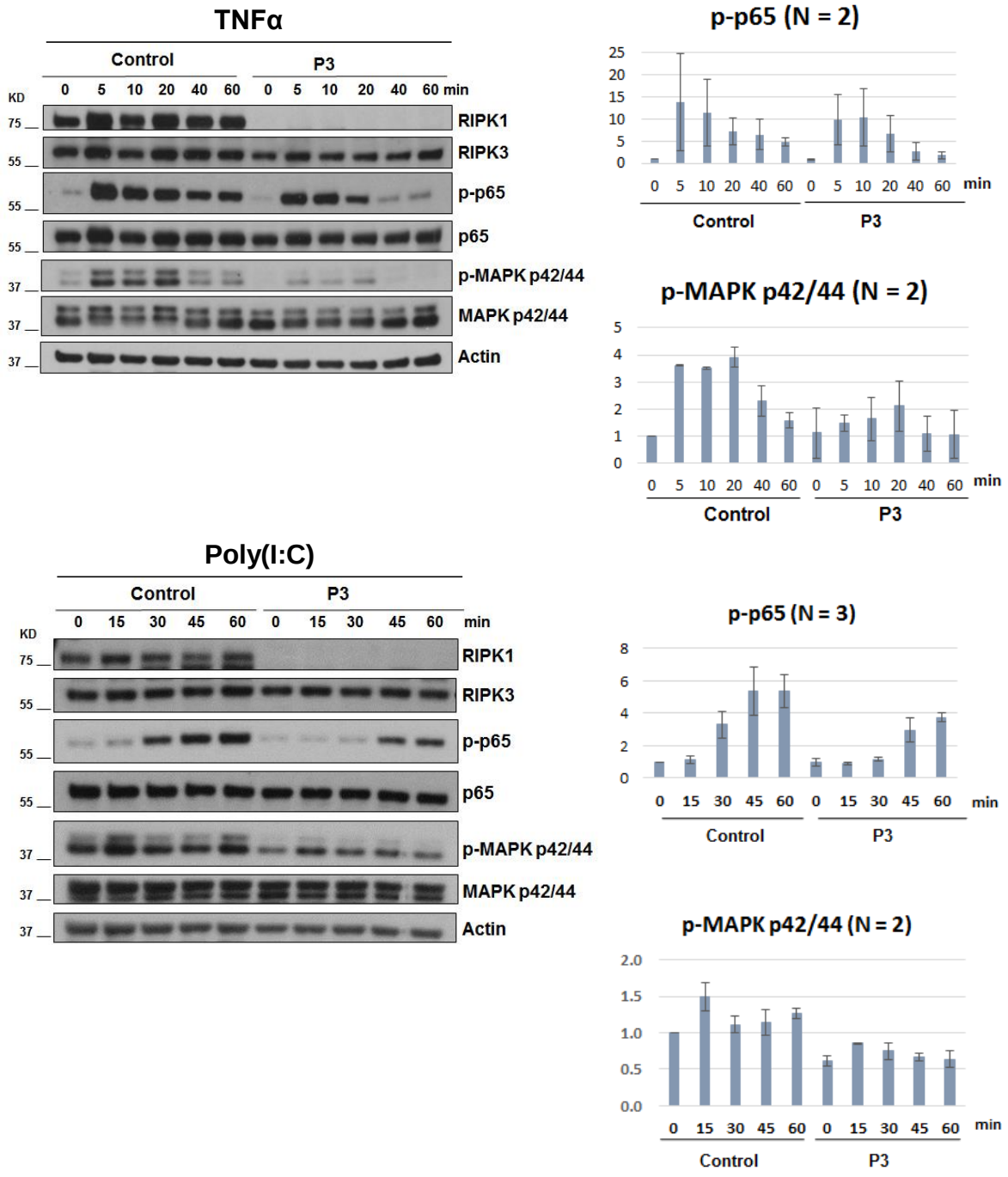

Fig. S6. RIPK1-deficient fibroblasts have partially reduced phosphorylation of MAPK p42/44 (ERK1/2) and p65 subunit of NF-κB

Primary fibroblasts were stimulated with 50 ng/mL TNFα or 100 μg/mL poly(I:C) and protein extracts were subjected to immunoblotting. Bar graphs show fold change of band densitometry. N shows the number of independent experiments. Graphs show mean values ± SD.

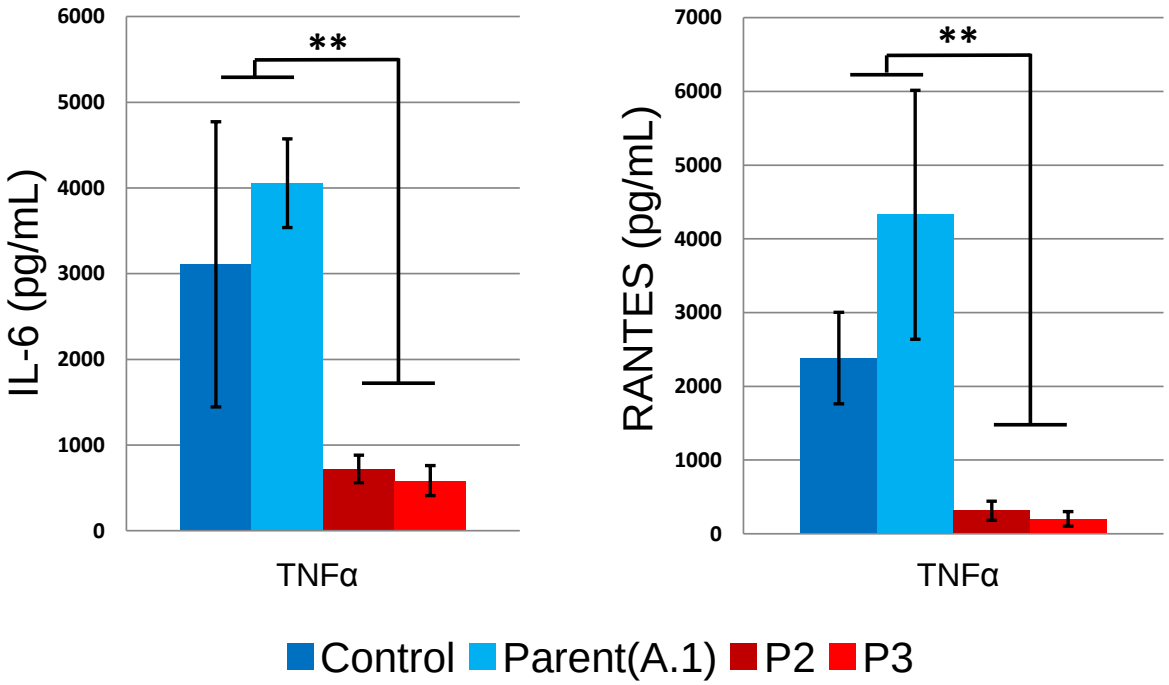

Fig. S7. RIPK1-deficient fibroblasts show reduced production of IL-6 and RANTES after TNFα stimulation

Primary fibroblasts of a healthy unrelated control, a healthy parent (A.1) and patients P2 and P3 were stimulated overnight with 100 ng/mL TNFα. Cytokines IL-6 and RANTES were measured in supernatants by ELISA (N=3). The data were corrected for the estimated number of live cells and show means ± SEM. *P*-values were calculated using two-tailed unpaired T-test. ** $P < 0.01$

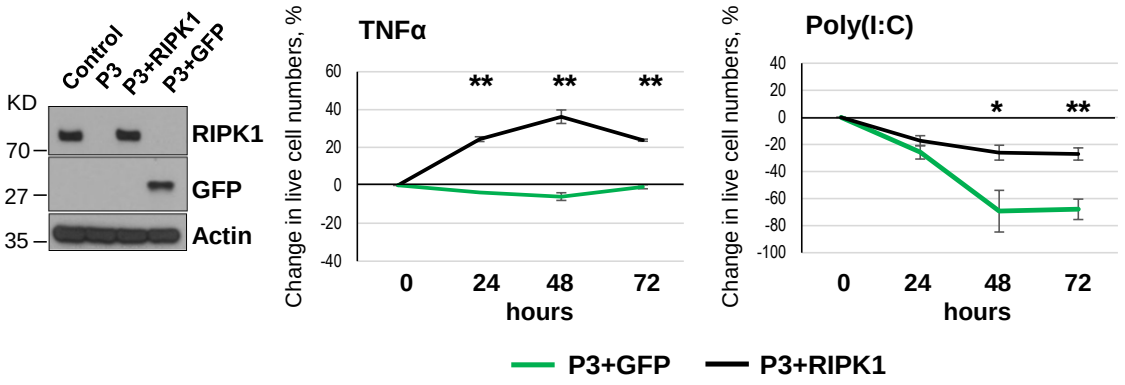

Fig. S8. **Forced expression of RIPK1 reverses viability defect in patient's fibroblasts**
Fibroblasts of P3 were transduced with lentiviral constructs expressing either RIPK1 or green fluorescent protein (GFP). Protein extracts were subjected to immunoblotting to determine levels of RIPK1 and GFP expression (left panel). Next, viability of the transduced fibroblasts was determined after stimulation with 50 ng/mL TNFα (center panel, N = 2) or 20 μg/mL poly(I:C) (right panel, N = 5). Differences between stimulated and unstimulated cells are shown at each time point relative to the 0 time point. *P*-values were calculated using two-tailed unpaired T-test; graphs show mean values ± SEM.
* $P < 0.05$, ** $P < 0.01$.

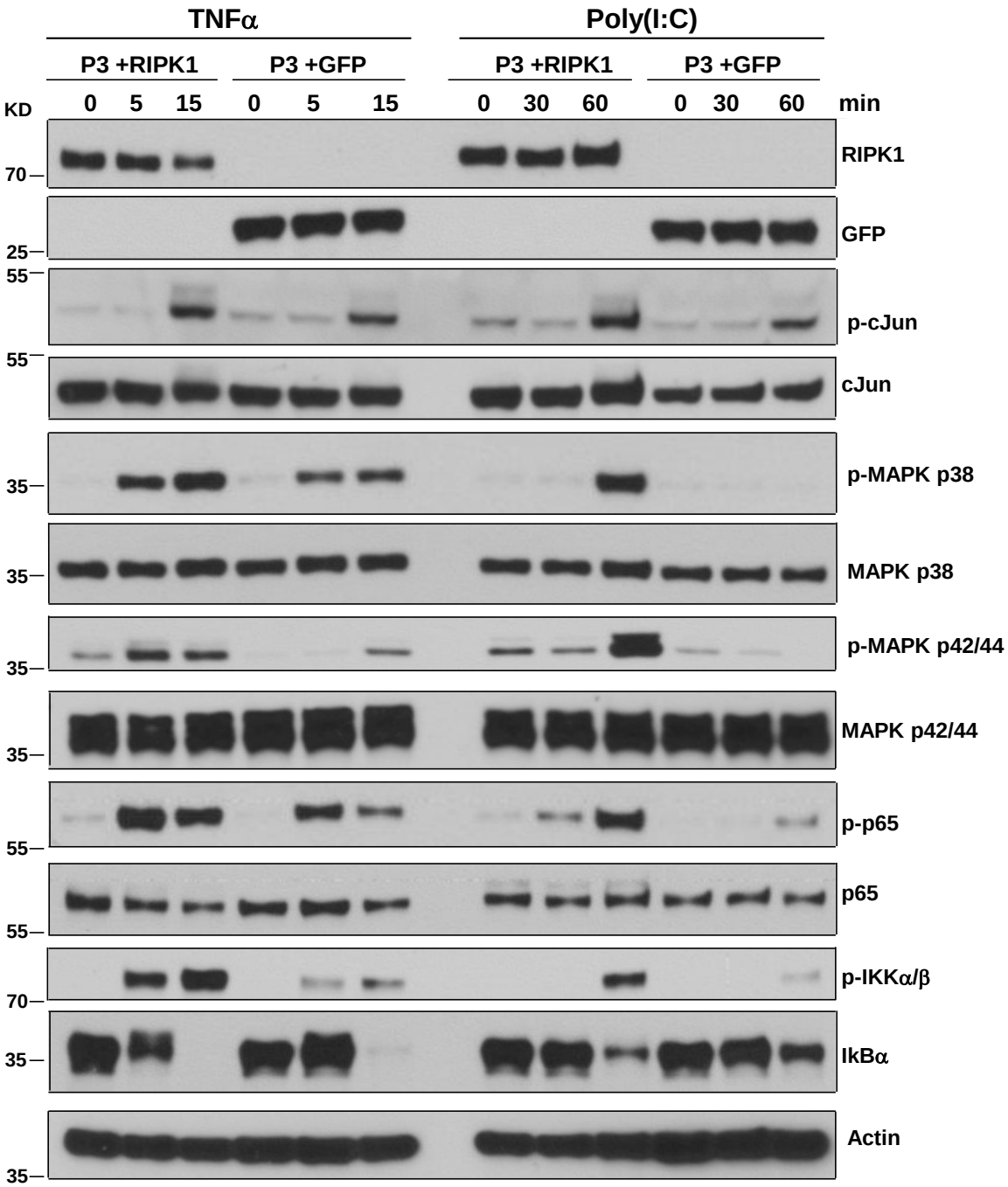

Fig. S9. Forced expression of RIPK1 rescues impaired MAPK and NF-κB activation in patient's fibroblasts

Fibroblasts of P3 were transduced with lentiviral constructs expressing either RIPK1 or green fluorescent protein (GFP). Next, cells were stimulated with 50 ng/mL TNFα or 100 μg/mL poly(I:C) for the indicated time and protein extracts were subjected to immunoblotting (N = 1).

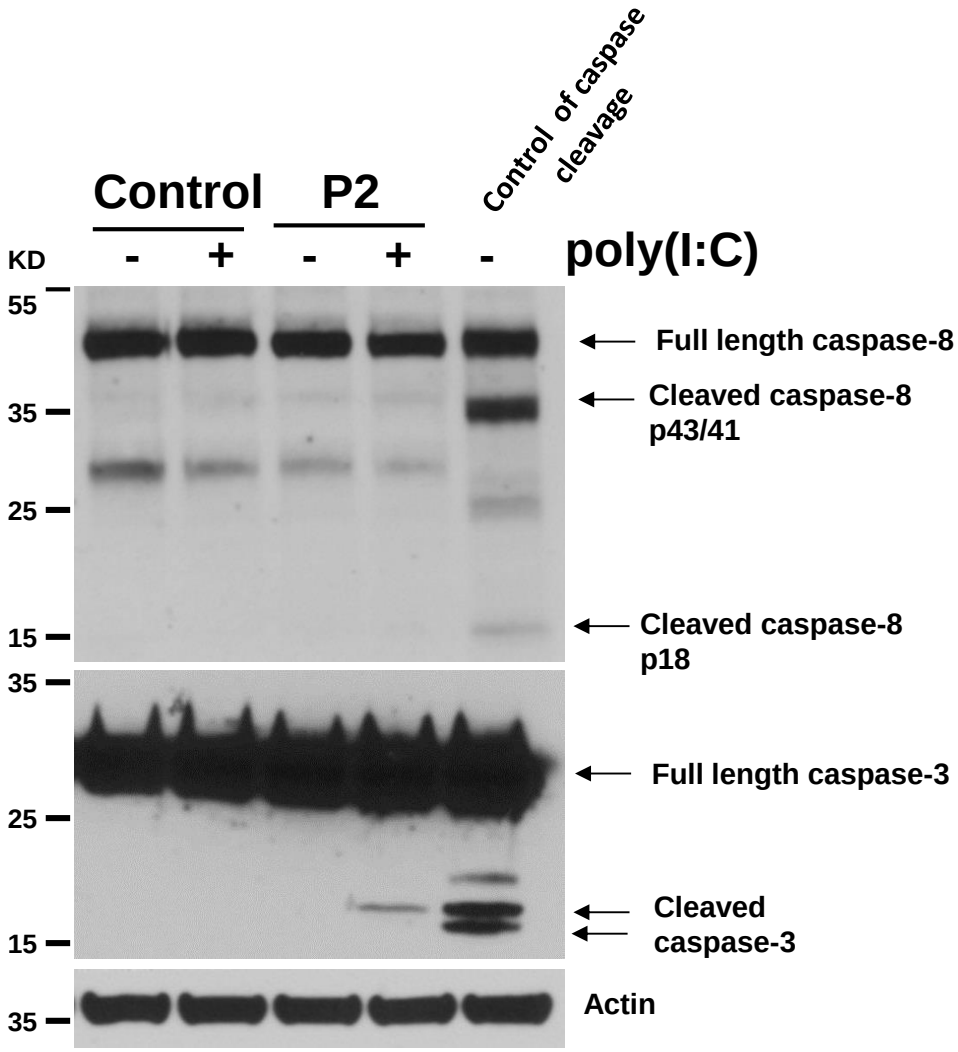

Fig. S10. Analysis of caspase-8 and caspase-3 cleavage in poly(I:C)-stimulated fibroblasts
Fibroblasts were stimulated with 20 μg/mL poly(I:C) for 24 hours and protein extracts were subjected to immunoblotting (N = 1). THP-1 cells stimulated with 50 μM of etoposide for 6 hours were used as a positive control of caspase cleavage.

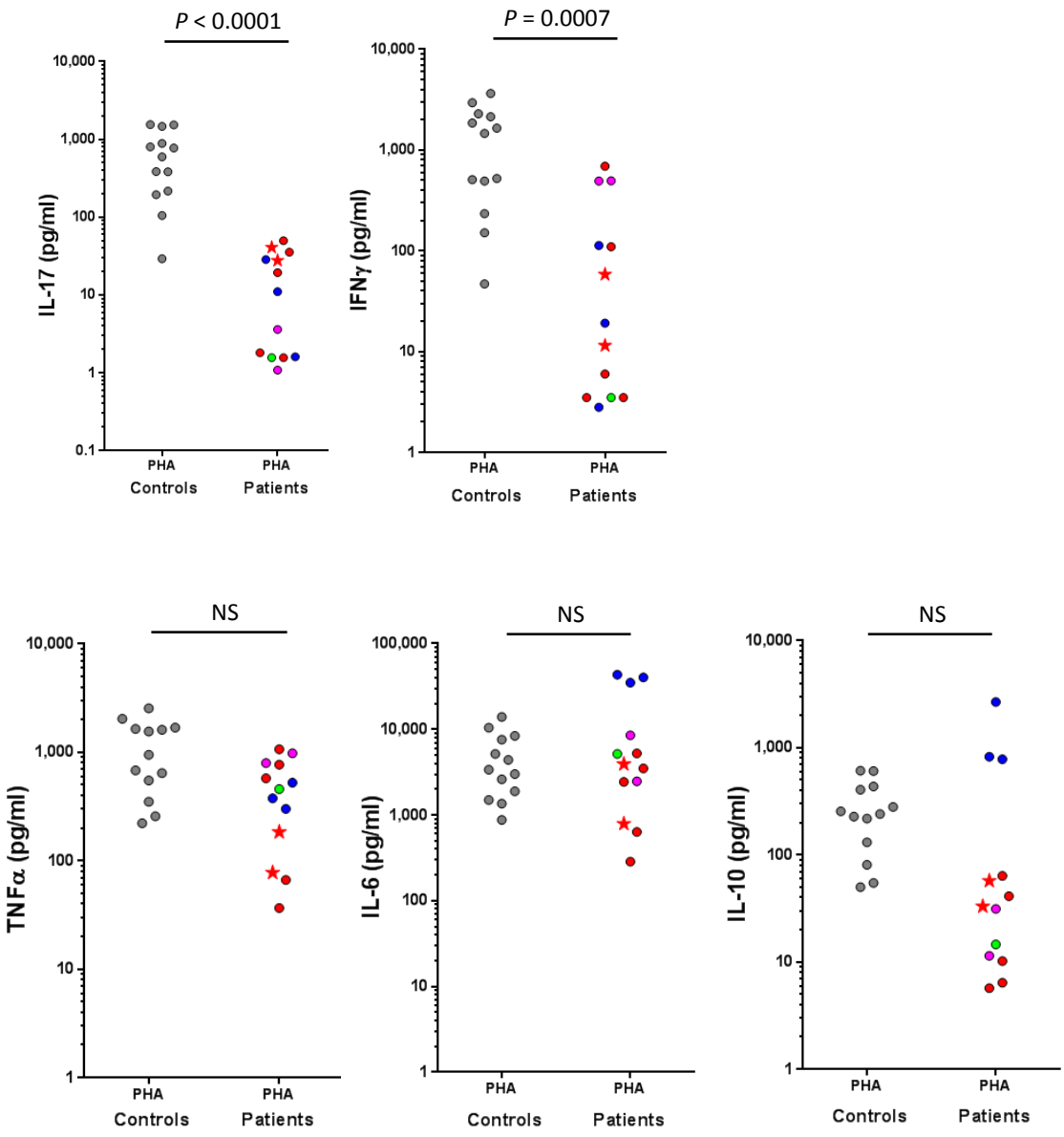

Fig. S11. **Cytokine production in whole blood after PHA stimulation**
Cytokine amounts were measured 24 hours after stimulation in whole blood of healthy controls (grey circles) and patients (colored circles: P1 – magenta, P3 – blue, P4 – green, P2 before HSCT – red; P2 after HSCT – red star). Stimulations were done using 10 µg/mL PHA. Data were normalized on lymphocyte counts to correct for lymphopenia. *P*-values were calculated using two-tailed Mann-Whitney test, excluding the data of P2 after HSCT.

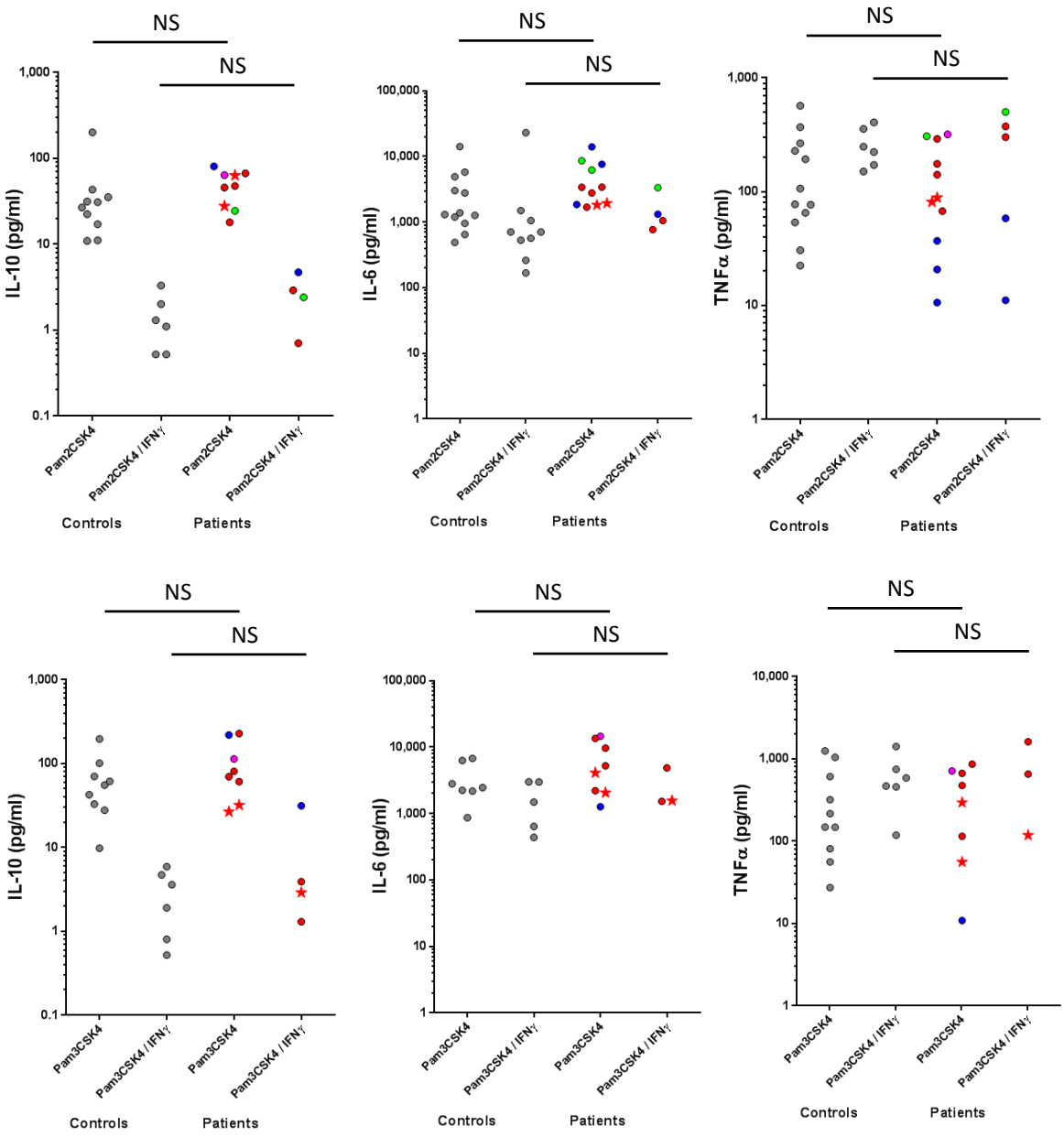

Fig. S12. Cytokine production in whole blood after Pam2CSK4 or Pam3CSK4 stimulation

Cytokine amounts were measured 24 hours after stimulation in whole blood of healthy controls (grey circles) and patients (colored circles: P1 – magenta, P3 – blue, P4 – green, P2 before HSCT – red; P2 after HSCT – red star). Stimulations were done using Pam2CSK4 (1 μg/mL) or Pam2CSK4 (1 μg/mL) plus IFN-γ (2 x 10^4 IU/mL), Pam3CSK4 (1 μg/mL) or Pam3CSK4 (1 μg/mL) plus IFN-γ (2 x 10^4 IU/mL). Data were normalized on lymphocyte counts to correct for lymphopenia. *P*-values were calculated using two-tailed Mann-Whitney test, excluding the data of P2 after HSCT.

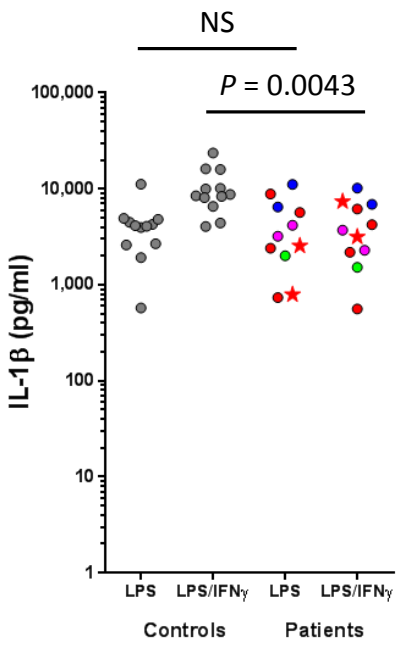

Fig. S13. IL-1β in whole blood after LPS stimulation
IL-1β was measured in whole blood after 24 hour stimulation using 1 μg/mL LPS or 1 μg/mL LPS plus 20,000 IU/mL IFN-γ. To account for lymphopenia data were corrected for lymphocyte counts. Controls are shown as grey circles, patients as colored circles (P1 – magenta, P3 – blue, P4 – green, P2 before HSCT – red; P2 after HSCT – red star). *P*-values were calculated using two-tailed Mann-Whitney test, excluding the data of P2 after HSCT.

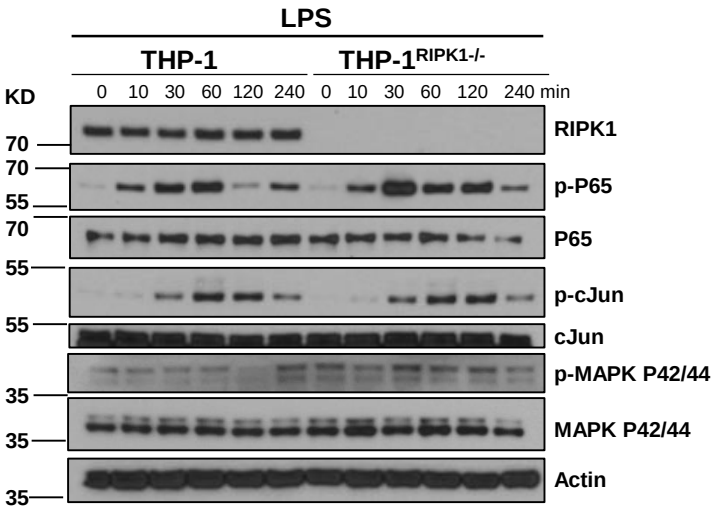

Fig. S14. RIPK1-deficient THP-1 cells have normal phosphorylation of MAPK p42/44 (ERK2/1) and p65 subunit of NF-κB

Wild-type THP-1 and THP-1$^{RIPK1-/-}$ cells (one clone each) were treated with 50 ng/mL PMA for 3 days, stimulated with 1 μg/mL LPS for the indicated time and the extracted proteins were analyzed by immunoblotting (N = 2).

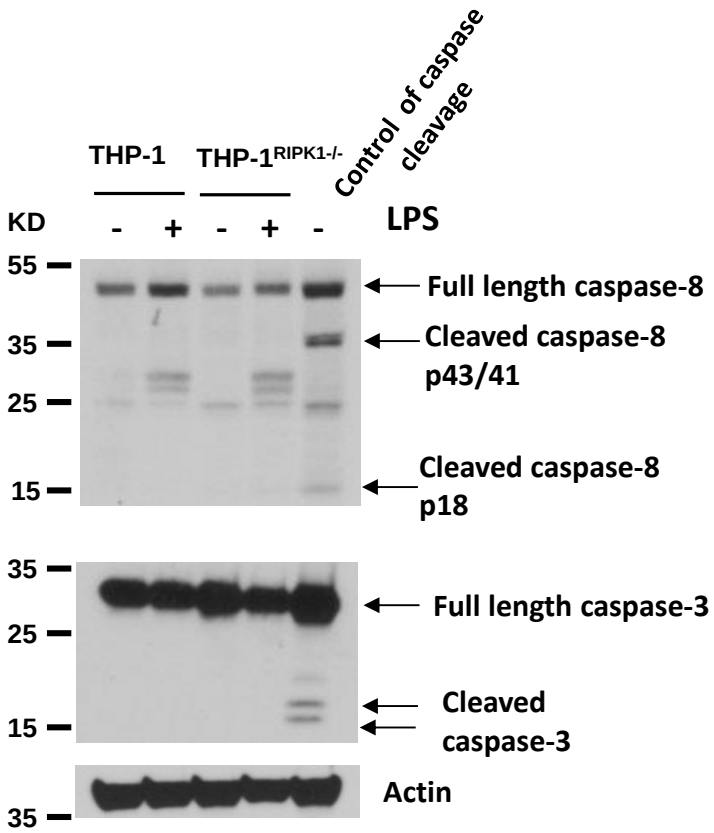

Fig. S15. **No caspase-8 and caspase-3 cleavage in LPS-stimulated THP-1 cells**
Wild-type THP-1 and THP-$1^{RIPK1-/-}$ cells (one clone each) were stimulated with 5 μg/mL LPS for 48 hours and the extracted proteins were analyzed by immunoblotting (N = 2). THP-1 cells stimulated with 50 μM of etoposide for 6 hours were used as a positive control of caspase cleavage.

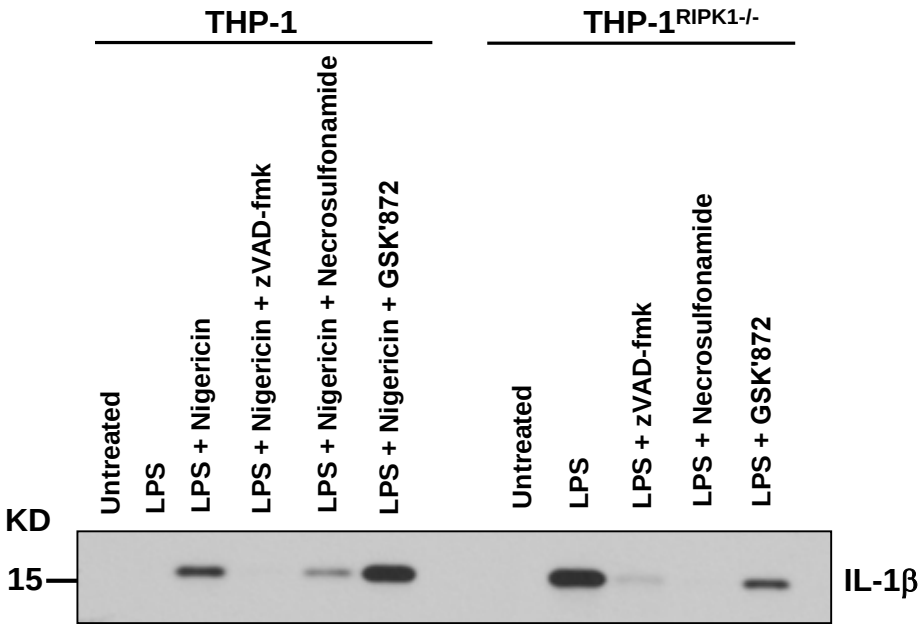

Fig. S16. IL-1β release during pyroptosis of wild-type THP-1 cells and necroptosis of THP-1$^{RIPK1-/-}$ cells

Wild-type THP-1 cells were stimulated with 5 μg/mL LPS for 48 hours and 20 μM Nigericin for the last 90 minutes in the presence of the indicated compounds. THP-1$^{RIPK1-/-}$ cells were stimulated with 5 μg/mL LPS for 48 hours in the presence of the indicated compounds. IL-1β was analysed in supernatants by immunoblotting (N = 1).

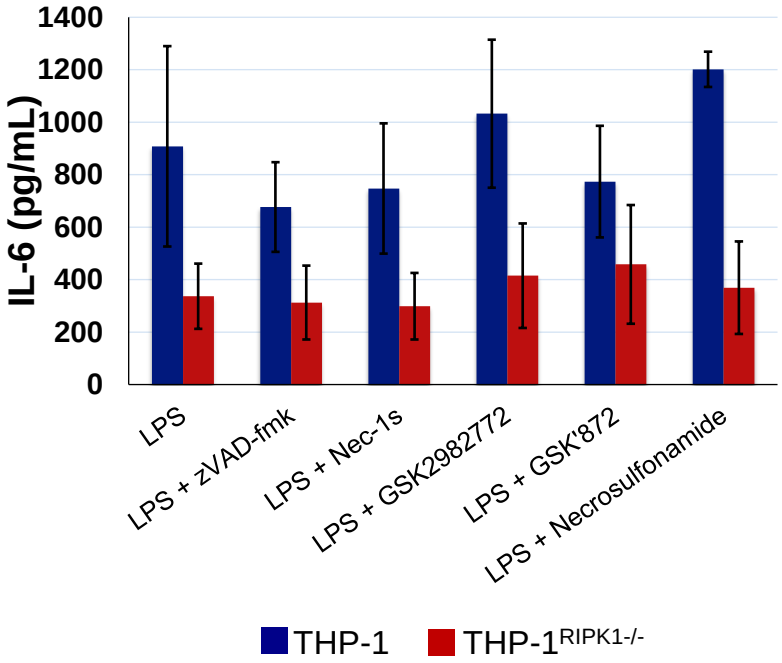

Fig. S17. Inhibitors of necroptosis do not rescue reduced IL-6 production in THP-1$^{RIPK1-/-}$ cells

Wild-type THP-1 (2 clones) and THP-1$^{RIPK1-/-}$ cells (4 clones) were stimulated with 5 µg/mL LPS for 24 hours in the presence of the indicated compounds. IL-6 was measured in supernatants by ELISA. *P*-values were calculated using two-tailed unpaired T-test; graphs show mean values ± SEM.

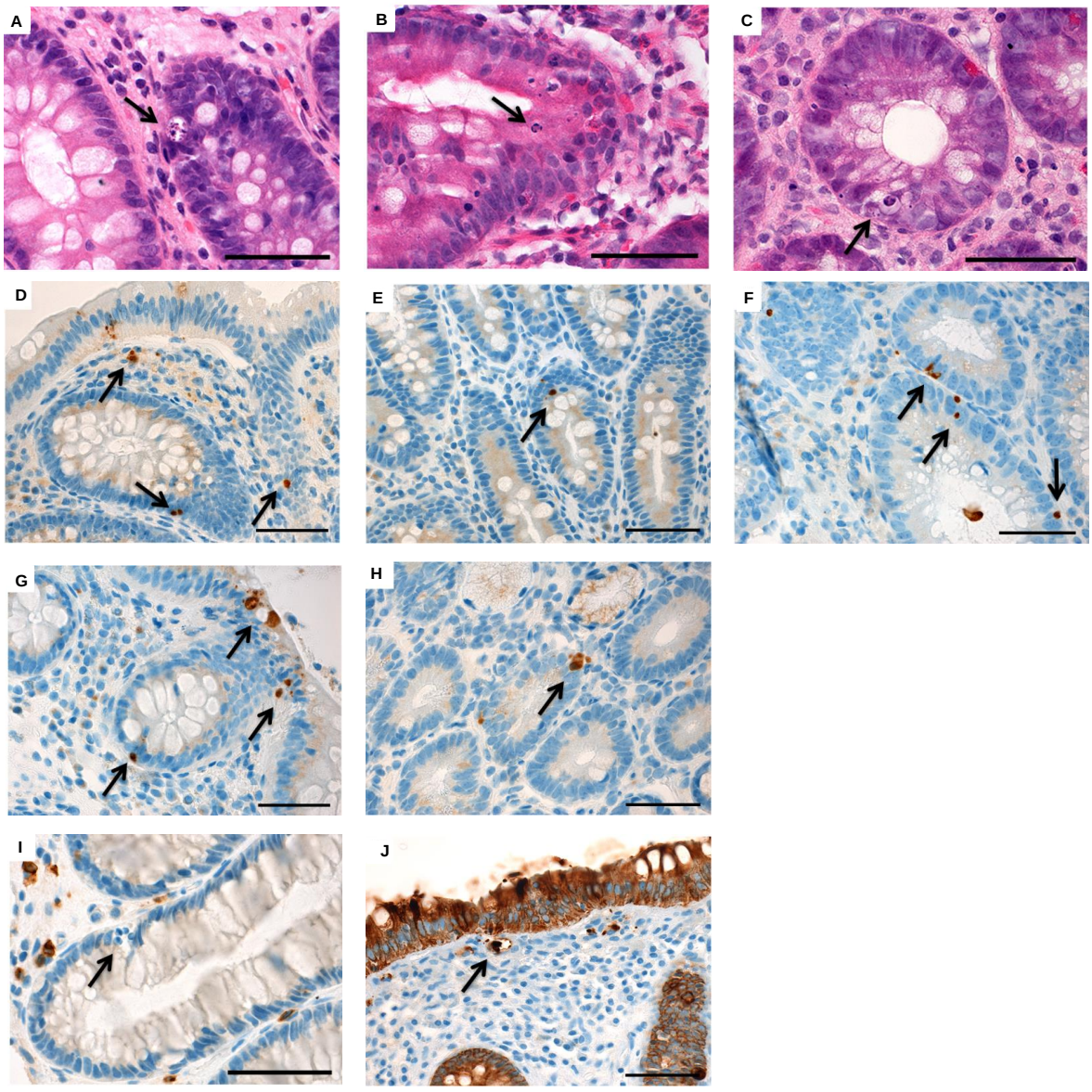

Fig. S18. Cell death in gastrointestinal biopsies from P1, P2 and controls
(A) An occasional epithelial cell with apoptotic morphology in colonic crypt epithelium of patient P1. Hematoxylin and eosin staining. Scale bar = 50 μm.
(B) An occasional epithelial cell with apoptotic morphology in duodenal crypt epithelium of patient P2. Hematoxylin and eosin staining. Scale bar = 50 μm.
(C) An occasional epithelial cell with apoptotic morphology in crypt epithelium of a colonic biopsy from a child with idiopathic inflammatory bowel disease. Hematoxylin and eosin staining. Scale bar = 50 μm.
(D) Immunostaining for cleaved caspase-3 showing occasional positive cells, including cells with apoptotic morphology, in the surface epithelium, lamina propria and crypt epithelium of the colon of patient P1. Scale bar = 50 μm.
(E) Immunostaining for cleaved caspase-3 showing an occasional positive cell in duodenal crypt epithelium of patient P2. Scale bar = 50 μm.

(F) Immunostaining for cleaved caspase-3 showing occasional positive cells in crypt epithelium of a colonic biopsy from a child with idiopathic inflammatory bowel disease. Scale bar = 50 μm.
(G) Immunostaining for cleaved caspase-3 showing occasional positive cells in the surface epithelium, lamina propria and crypt epithelium of a histologically normal colonic biopsy. Scale bar = 50 μm.
(H) Immunostaining for cleaved caspase-3 showing an occasional positive cell in crypt epithelium of a histologically normal duodenal biopsy. Scale bar = 50 μm.
(I) Immunostaining for CD3 showing negativity of an apoptotic colonic crypt epithelial cell of patient P1. Scale bar = 50 μm.
(J) Immunostaining for cytokeratin showing positive staining of apoptotic cells and apoptotic bodies in the superficial colonic lamina propria of patient P1. Together with (I) this indicates epithelial origin of the apoptotic cells. Scale bar = 50 μm.

References and notes:

1. A. Bousfiha *et al.*, The 2017 IUIS Phenotypic Classification for Primary Immunodeficiencies. *J Clin Immunol* **38**, 129 (2018).
2. Materials and Methods are available as Supplementary Materials.
3. M. Lek *et al.*, Analysis of protein-coding genetic variation in 60,706 humans. *Nature* **536**, 285 (2016).
4. D. Ofengeim, J. Yuan, Regulation of RIP1 kinase signalling at the crossroads of inflammation and cell death. *Nat Rev Mol Cell Biol* **14**, 727 (2013).
5. M. Pasparakis, P. Vandenabeele, Necroptosis and its role in inflammation. *Nature* **517**, 311 (2015).
6. M. Najjar *et al.*, RIPK1 and RIPK3 Kinases Promote Cell-Death-Independent Inflammation by Toll-like Receptor 4. *Immunity* **45**, 46 (2016).
7. M. A. Kelliher *et al.*, The death domain kinase RIP mediates the TNF-induced NF-kappaB signal. *Immunity* **8**, 297 (1998).
8. J. A. Rickard *et al.*, RIPK1 regulates RIPK3-MLKL-driven systemic inflammation and emergency hematopoiesis. *Cell* **157**, 1175 (2014).
9. M. Dannappel *et al.*, RIPK1 maintains epithelial homeostasis by inhibiting apoptosis and necroptosis. *Nature* **513**, 90 (2014).
10. T. H. Lee *et al.*, The death domain kinase RIP1 is essential for tumor necrosis factor alpha signaling to p38 mitogen-activated protein kinase. *Mol Cell Biol* **23**, 8377 (2003).
11. E. Meylan *et al.*, RIP1 is an essential mediator of Toll-like receptor 3-induced NF-kappa B activation. *Nat Immunol* **5**, 503 (2004).
12. D. W. Zhang *et al.*, RIP3, an energy metabolism regulator that switches TNF-induced cell death from apoptosis to necrosis. *Science* **325**, 332 (2009).
13. L. Sun *et al.*, Mixed lineage kinase domain-like protein mediates necrosis signaling downstream of RIP3 kinase. *Cell* **148**, 213 (2012).
14. R. A. Gottschalk *et al.*, Distinct NF-kappaB and MAPK Activation Thresholds Uncouple Steady-State Microbe Sensing from Anti-pathogen Inflammatory Responses. *Cell Syst* **2**, 378 (2016).
15. K. Newton *et al.*, Activity of protein kinase RIPK3 determines whether cells die by necroptosis or apoptosis. *Science* **343**, 1357 (2014).
16. A. Polykratis *et al.*, Cutting edge: RIPK1 Kinase inactive mice are viable and protected from TNF-induced necroptosis in vivo. *J Immunol* **193**, 1539 (2014).
17. W. J. Kaiser *et al.*, RIP1 suppresses innate immune necrotic as well as apoptotic cell death during mammalian parturition. *Proc Natl Acad Sci U S A* **111**, 7753 (2014).
18. J. E. Roderick *et al.*, Hematopoietic RIPK1 deficiency results in bone marrow failure caused by apoptosis and RIPK3-mediated necroptosis. *Proc Natl Acad Sci U S A* **111**, 14436 (2014).
19. A. Degterev *et al.*, Chemical inhibitor of nonapoptotic cell death with therapeutic potential for ischemic brain injury. *Nat Chem Biol* **1**, 112 (2005).
20. H. Zhao *et al.*, Role of necroptosis in the pathogenesis of solid organ injury. *Cell Death Dis* **6**, e1975 (2015).
21. M. M. Gaidt *et al.*, Human Monocytes Engage an Alternative Inflammasome Pathway. *Immunity* **44**, 833 (2016).

22. B. N. Martin *et al.*, T cell-intrinsic ASC critically promotes T(H)17-mediated experimental autoimmune encephalomyelitis. *Nat Immunol* **17**, 583 (2016).
23. G. Arbore *et al.*, T helper 1 immunity requires complement-driven NLRP3 inflammasome activity in CD4(+) T cells. *Science* **352**, aad1210 (2016).
24. G. Schett, J. M. Dayer, B. Manger, Interleukin-1 function and role in rheumatic disease. *Nat Rev Rheumatol* **12**, 14 (2016).
25. M. F. Neurath, Cytokines in inflammatory bowel disease. *Nat Rev Immunol* **14**, 329 (2014).
26. R. Kuhn, J. Lohler, D. Rennick, K. Rajewsky, W. Muller, Interleukin-10-deficient mice develop chronic enterocolitis. *Cell* **75**, 263 (1993).
27. E. O. Glocker *et al.*, Inflammatory bowel disease and mutations affecting the interleukin-10 receptor. *N Engl J Med* **361**, 2033 (2009).
28. B. Khor, A. Gardet, R. J. Xavier, Genetics and pathogenesis of inflammatory bowel disease. *Nature* **474**, 307 (2011).
29. N. Takahashi *et al.*, RIPK1 ensures intestinal homeostasis by protecting the epithelium against apoptosis. *Nature* **513**, 95 (2014).
30. J. Lin *et al.*, RIPK1 counteracts ZBP1-mediated necroptosis to inhibit inflammation. *Nature* **540**, 124 (2016).
31. The 1000 Genomes Project Consortium, An integrated map of genetic variation from 1,092 human genomes. *Nature* **491**, 56 (2012).
32. W. Fu *et al.*, Analysis of 6,515 exomes reveals the recent origin of most human protein-coding variants. *Nature* **493**, 216 (2013).
33. V. Plagnol *et al.*, A robust model for read count data in exome sequencing experiments and implications for copy number variant calling. *Bioinformatics* **28**, 2747 (2012).
34. C. Zheng, B. J. Baum, All human EF1alpha promoters are not equal: markedly affect gene expression in constructs from different sources. *Int J Med Sci* **11**, 404 (2014).
35. E. J. Schatorje *et al.*, Paediatric reference values for the peripheral T cell compartment. *Scand J Immunol* **75**, 436 (2012).